Transactions

of the I·R·E

Professional Group on Antennas and Propagation

Paul Weaver

2
VOLUME AP[illegible] NUMBER 4 OCTOBER 1954

Published Quarterly

news and views Page 129

contributions

Analysis of Helical Transmission Lines by Means of the Complete Circuit Equations
Vernon J. Fowler Page 132

Radiation from a Vertical Dipole over a Stratified Ground (Part II)
J. R. Wait and W. C. G. Fraser Page 144

A Waveguide Array for Solar Noise Studies
H. Gruenberg Page 147

Dielectric Sheet Radiators
F. E. Butterfield Page 152

Evaluation of Errors in an Eight-Element Adcock Antenna
J. R. Wait and W. A. Pope Page 159

communications

An Exact Step-Up Impedance-Ratio Chart of a Folded Antenna
Yasuto Mushiake Page 163

index

Volume AP-2—1954 (Cross-referenced) Page 164

7800
2
.2

The Institute of Radio Engineers

ADMINISTRATIVE COMMITTEE

D. C. Ports, *Chairman*
H. G. Booker, *Vice-Chairman*
R. L. Mattingly, *Secretary-Treasurer*

J. T. Bolljahn
J. S. Brown
H. A. Finke
R. A. Helliwell

V. H. Rumsey
George Sinclair
J. B. Smyth

R. C. Spencer
A. W. Straiton
L. C. Van Atta
H. W. Wells

EX OFFICIO MEMBERS

P. S. Carter
A. H. Waynick

TRANSACTIONS OF THE I•R•E® PGAP IS A QUARTERLY PUBLICATION DEVOTED TO EXPERIMENTAL AND THEORETICAL PAPERS ON ANTENNAS AND WIRELESS PROPAGATION OF ELECTROMAGNETIC WAVES

MANUSCRIPTS should be submitted to John B. Smyth, Editor, U. S. Navy Electronics Laboratory, San Diego, California. Manuscripts should be original typewritten copy, double spaced, plus one carbon copy. References should appear as footnotes and include author's name, title, journal, volume, initial and final page numbers, and date. Each paper must have an abstract of not more than 200 words. News items concerning PGAP members and group activities should be sent to the News Editor, Mr. H. A. Finke, Polytechnic Research and Development Company, 55 Johnson Street, Brooklyn, New York.

ILLUSTRATIONS should be submitted as follows: All line drawings (graphs, charts, block diagrams, cutaways, etc.) should be inked uniformly and ready for reproduction. If commercially printed grids are used in graph drawings, author should be sure printer's ink is of a color that will reproduce. All half-tone illustrations (photographs, wash, airbrush, or pencil renderings, etc.) should be clean and ready to reproduce. Photographs should be glossy prints. Call-outs or labels should be marked on a registered tissue overlay, not on the illustration itself. No illustration should be larger than 8 x 10 inches.

UNIVERSITY OF HAWAII
LIBRARY
NOV 4 1 38 PM '77

Copies can be purchased from
THE INSTITUTE OF RADIO ENGINEERS
1 East 79 St., New York 21, N.Y.

PRICE PER COPY: members of the Professional Group on Antennas and Propagation $1.50; members of the IRE $2.25; nonmembers $4.50.

Copyright 1954, by The Institute of Radio Engineers, Inc.

Entered as second-class matter, at the post office at Menasha, Wisconsin, under the act of August 24, 1912. Acceptance for mailing at a special rate of postage is provided for in the act of February 28, 1925, embodied in Paragraph 4, Section 412, P. L. & R., authorized October 26, 1927.

news and views

PGAP Administrative Committee Meeting at WESCON

A MEETING of the Administrative Committee was held at the Ambassador Hotel, Los Angeles, during the WESCON convention. Delmer Ports, newly appointed chairman of the group, presided.

The Transactions was the major subject of the three-hour meeting and various comments were offered concerning the future course of our quarterly. There is a surprising amount of policy that has yet to be established, much of which, however, may well solve itself. The scope of the Transactions is open to question. Should papers on microwaves components appear? Should good articles on radio astronomy be included in our scope? Should technical papers of foreign authors be solicited? The question of some special handling of student papers was raised but was not too favorably received. It would be very helpful to the Administrative Committee if the membership were to express themselves on these subjects in the form of correspondence to the News and Views Editor.

Another very important issue was reviewed—the problem of how to make the Transactions the initial clearing house for papers in the Antenna and Propagation fields. Currently, most IRE papers go to IRE headquarters for evaluation. It seems logical that PGAP, as the most cognizant technical group, should be in the best position to evaluate initially the disposition of technical contributions. This is a matter that will be taken up with IRE. Authors, too, could well consider the desirability of initial presentation of their papers in the PGAP Transactions. The problem of control of papers that are sent elsewhere than to the IRE was also considered, but the solution to this probably lies only in authors cooperating with their own professional group technical organ.

In general, considerable satisfaction was expressed with the progress of the past year, but it was recognized that a dynamic and forceful approach was still necessary in this period of growth of the Transactions.

A. W. Straiton was appointed Chairman of the Papers Procurement Committee for the coming year, and a Vice-Chairman will shortly be named by Delmer Ports.

Publication of papers delivered at the WESCON convention was considered and it was agreed that authors would be requested to organize their material in a form suitable for publication. These papers would then be subjected to the same technical screening as any other contributions and, if accepted, an acknowledgement of the WESCON presentation would appear, probably as a footnote.

Delmer Ports read off a brief summary of the financial circumstances of the PGAP as of June 30, 1954. Our balance as of January 1 was $6,033.14. Between January 1 and June 30 we derived an income of $3,644.65. This income came from membership assessments, IRE matching funds, advertising, and sale of publications. Our expenses during the same six month period were $4,071.63. Most of this was for publication of the Transactions, with a very small amount due to sundry service charges. Our net balance as of June 30 is, then, $5,606.16.

Combining of Professional Groups

Dr. W. R. G. Baker, Chairman of the Professional Groups Committee, has recently created a Task Force under Dr. Ernst Weber to determine any tendencies of the Professional Groups to combine or dissociate further. The Committee consists of the following personnel: J. L. Callahan—Communications Systems and Vehicular Communications; A. G. Clavier—Microwave Theory & Techniques and Component Parts; H. A. Finke—Antennas & Propagation and Nuclear Science; A. A. Gerlach—Audio and Ultrasonics Engineering; A. W. Graf—Engineering Management and Industrial Electronics; R. A. Heising—Aeronautical & Navigational Electronics and Radio Telemetry & Remote Control; W. E. Noller—Broadcast & TV Receivers and Broadcast Transmission Systems; G. D. O'Neill—Electron Devices, Quality Control and Production Techniques; E. Weber—Instrumentation, Circuit Theory and Medical Electronics; and J. R. Weiner—Electronic Computers and Information Theory.

A meeting of this Task Force was held on July 21 at IRE Headquarters, and views of members were presented. Further discussion will be necessary; it is too early for positive conclusions. However, the general trend of thinking seems to be to permit the Professional Groups to work out their own problems, that those groups that feel the desirability of consolidation or other reorganization should further explore such problems, and that, in general, final decisions should not be made by any group until its membership has been carefully consulted. Further information on the discussions of this Task Force will be reported upon as available.

RELOCATION OF THE CENTRAL RADIO PROPAGATION LABORATORY OF THE NATIONAL BUREAU OF STANDARDS

About 150 employees of the Central Radio Propagation Laboratory (CRPL), National Bureau of Standards, and their families, have been moved from their present location at the Bureau in Washington to new quarters in Boulder, Colorado. They are occupying a new four-million-dollar building.

This group joined approximately 80 additional employees of the CRPL who had been working in temporary quarters in Boulder for the past three years. Other employees are being recruited to replace staff lost by the move. This building also affords facilities and space to accommodate an administrative staff for this second major center of the National Bureau of Standards.

The Boulder Laboratories are actively planning to develop this new location as an important scientific center. Prominent scientists in the fields of radio wave propagation and radio communications will be invited to join the staff as guest workers or to participate in special colloquia. Major efforts will be made to attract national and international scientific societies and organizations to hold meetings at the Boulder Laboratories.

ADMINISTRATIVE COMMITTEE ADDITIONS

In the last issue of the TRANSACTIONS we reported a number of nominations to the PGAP Administrative Committee. These nominations were submitted to balloting by the entire membership, and we now take pleasure in announcing the results of the poll. The newly elected committee members are: R. A. Helliwell, V. H. Rumsey, R. C. Spencer, and A. W. Straiton. We wish them every success.

IRE PROFESSIONAL GROUP DATA

In the course of generating some data on Professional Group composition and activity this chart was prepared.

Code	Title	Membership May 31, 1954		Assessment	TRANSACTIONS 1951–1952		TRANSACTIONS 1953		No. of Local Chapters
		Paid	Unpaid		Total No. of Issues	Total No. of Papers	Total No. of Issues	Total No. of Papers	
G-1	Audio	2359	18	$2.00	10	33	6	23	14
G-2	Broadcast Transmission Systems	741	499	2.00	—	—	—	—	4
G-3	Antennas and Propagation	1268	1	4.00	4	100	2	12	3
G-4	Circuit Theory	2440	853	2.00	1	7	1	9	5
G-5	Nuclear Science	566	1272	2.00	—	—	—	—	7
G-6	Vehicular Communications	643	3	2.00	2	18	1	14	6
G-7	Quality Control	506	328	2.00	1	6	1	5	1
G-8	Broadcast and Television Receivers	1274	6	2.00	1	1	3	15	2
G-9	Instrumentation	2133	5	1.00	1	5	1	13	3
G-10	Radio Telemetry and Remote Control	987	948	1.00	—	—	—	—	3
G-11	Aeronautical and Navigational Electronics	1565	27	2.00	6	8	4	17	6
G-12	Information Theory	1339	418	2.00	—	—	1	36	3
G-13	Industrial Electronics	988	1344	2.00	—	—	1	6	1
G-14	Engineering Management	1479	647	1.00	—	—	—	—	6
G-15	Electron Devices	1267	27	2.00	1	5	3	16	7
G-16	Electronic Computers	2566	53	2.00	—	—	4	15	11
G-17	Microwave Theory & Techniques	1337	326	2.00	—	—	2	20	4
G-18	Medical Electronics	868	303	1.00	—	—	1	2	3
G-19	Communications Systems	853	480	2.00	—	—	1	11	1
G-20	Ultrasonics Engineering	237	140	—	—	—	—	—	0
G-21	Component Parts	365	232	—	—	—	—	—	4
G-22	Production Techniques	—	40	—	—	—	—	—	0
	Totals	25,781	7970		27	183	32	214	94

GROUP CHAPTERS AND CHAPTER NEWS

Chicago Chapter

This PGAP Chapter had an active and productive year during 1953–1954, according to the outgoing Chairman, George Kearse. A total of six meetings were held and six papers were presented, with Mr. L. R. Krahe as Program Chairman. The following talks were held at the last two meetings:

March 19, 1954—"UHF TV Propagation Problems," by Mr. H. N. Frihart, Motorola.

Mr. Frihart presented a theoretical analysis of calculated field strengths of TV signals throughout the UHF range. These were then compared with the calculated values for the VHF ranges, and curves were shown which more clearly displayed the differences in propagation between the two. The data was compared to field reports from observers in several different sections of the country.

March 19, 1954—"TV Receiving Distribution Systems," by Mr. Irving Kaluzna, I. J. Kayle and Assoc.

Mr. Kaluzna detailed the problems encountered in laying out an apartment house TV distribution system. Calculation of losses in the cable runs and coupling transformer for a typical installation was shown and the selection of suitable broadband amplifiers and antenna systems was discussed. The application of distribution techniques to outdoor community systems and some of the problems encountered were also discussed.

May 21, 1954—"Ferrites," by Mr. E. H. Turner, Bell Labs.

Mr. Turner gave a detailed analysis of the molecular action within ferrite materials under the influence of an external magnetic field. This effect proved advantageous in the design of directional couplers at microwave frequencies. Several directional couplers were described using this principle.

ELECTION OF OFFICERS

The following officers for the next year were elected at the April meeting: L. R. Krahe, *Chairman;* R. A. Jensen, *Vice-Chairman;* and W. F. Mrazek, *Secretary.*

PERSONALS

Dr. E. C. Jordan of the University of Illinois has been nominated Dean of Engineering at the University of Illinois.

Dr. M. M. Newman of Lightning and Transients Research Institute, Minneapolis, Minn. is on an extended trip to Africa.

Dr. Rodolfo M. Soria has been appointed Director of Engineering of the American Phenolic Corporation. He succeeds Richard M. Purinton, recently resigned Vice-President, who is now representing the company in the New England area. Dr. Soria, formerly head of the Amphenol Development Division, now assumes full responsibility for the administration of all Amphenol engineering functions. Dr. Soria joined Amphenol in August, 1946. He is a graduate of MIT with a BS and Master's degrees. He received his Ph.D. from the Illinois Institute of Technology. Prominent in IRE affairs, he is the 1954 President of the National Electronics Conference.

The Yale Engineering Association has honored Dr. Seymour Cohn, head of the Microwave Group in SRI's Radio Systems Laboratory, with its 1954 Award for Advancement of Basic and Applied Science. The award is made annually to "A young man with an outstanding record in advancing our knowledge of the basic and applied sciences." Presentation was made at the Association's annual dinner in New York City, May 6.

Dr. Cohn became a member of the SRI staff early in 1953. His group is engaged in research and development of microwave equipment.

He received the Lamphier Award, a recognition of achievement and ability for senior students, at the time of his graduation from Yale University. During World War II he was a special research associate at Harvard University's Radio Research Laboratory. After leaving the Laboratory he continued studies at Harvard on a fellowship granted by the National Research Council. In 1948 he received a Ph.D. in Engineering Science and Applied Physics. As a project engineer, and later a research engineer with Sperry Gyroscope Co. at Great Neck, N. Y., he worked on waveguide devices, microwave circuits, and antennas.

He is the author of several chapters on uhf and microwave filters in the book, "Very High Frequency Techniques," written by members of the Radio Research Lab., and has had fifteen papers published in technical journals.

* * *

contributions

Analysis of Helical Transmission Lines by Means of the Complete Circuit Equations*

VERNON J. FOWLER†

Summary—**A set of integro-differential equations, called the "complete circuit equations," are derived from Maxwell's equations and applied to the solution of the parallel-wire transmission line, the double-helix transmission line, and the single helix, or helical waveguide. These equations take into account the effects of inductance and capacitance distribution, retardation, and outward radiation. A generalization of earlier concepts of distributed inductance and elastance (or inverse capacitance) is manifest in the solution of the helical line, where these quantities become functions of the phase coefficient or wavelength of propagation and are Fourier transforms of certain closed-form distribution functions. In general, phase velocity is a complicated implicit function of frequency, but under a hypothesis of "mode segregation on the basis of wavelength" the phase velocity and frequency can be obtained parametrically in terms of a third variable, called the phase parameter. Using this hypothesis, plots of phase velocity and characteristic impedance versus frequency were obtained for the double helix and the helical waveguide.**

DERIVATION OF THE COMPLETE CIRCUIT EQUATIONS FROM MAXWELL'S EQUATIONS

CIRCUITAL relationships are generally expressed in terms of currents and voltages which are well defined only for slowly varying fields. However, these quantities have alternative expressions which are almost as universally applicable as the electric and magnetic field intensities themselves: namely, the current density ι and the scalar electric potential ϕ. The circuital relationships that are to be considered in this paper find their most exact expression in terms of these two quantities.

Most of the preliminary definitions and analysis leading to the complete circuit equations are given in the literature[1,2] and will not be repeated here. For homogeneous isotropic media, the magnetic flux density B and the electric intensity E can be expressed in terms of a vector magnetic potential A and a scalar electric potential, ϕ as follows:

$$B = \nabla \times A \tag{1}$$

$$E = -\nabla\phi - \frac{\partial A}{\partial t}. \tag{2}$$

The divergence of A can be specified arbitrarily, thereby completing the definitions of A and ϕ as unique quantities. By letting

$$\nabla \cdot A = -\mu\epsilon\frac{\partial\phi}{\partial t} \tag{3}$$

the two wave equations in A alone and in ϕ alone are obtained,

$$\nabla^2 A - \mu\epsilon\frac{\partial^2 A}{\partial t^2} = -\mu\iota \tag{4}$$

$$\nabla^2\phi - \mu\epsilon\frac{\partial^2\phi}{\partial t^2} = -\frac{\rho}{\epsilon}. \tag{5}$$

These can be integrated directly by Kirchoff's method.[3]

---

* Revised manuscript received by the PGAP, May 17, 1954; received by the IRE, July 7, 1953. Sponsored by Air Force Cambridge Res. Center, Contract AF 19(604)-524.

† Res. Asst., Electron Tube Lab., Univ. of Illinois, Urbana, Ill.

[1] S. Ramo and J. R. Whinnery, "Fields and Waves in Modern Radio," John Wiley and Sons, New York, N. Y.; 1948.

[2] J. A. Stratton, "Electromagnetic Theory," McGraw-Hill Book Company, Inc., New York, N. Y.; 1941.

[3] Stratton, *op. cit.*, chap. 8, pp. 424–431.

$$A = \frac{\mu}{4\pi}\int_{\Omega} \frac{\iota\left(t - \dfrac{r}{c}\right) d\Omega}{r} \tag{6}$$

$$\phi = \frac{1}{4\pi\epsilon}\int_{\Omega} \frac{\rho\left(t - \dfrac{r}{c}\right) d\Omega}{r} \tag{7}$$

where

$$c = \frac{1}{\sqrt{\mu\epsilon}} \tag{8}$$

and Ω denotes a closed domain, bounded by a regular surface, containing all sources which contribute to the field.

In the practical application of these potentials, the condition of homogeneity is commonly violated by the presence in the medium of conductors in and on which flows the current ι. However, since the actual current distribution in the conductors is not sought for its own sake, it suffices to regard ι as an equivalent current distribution in the medium displaced by the conductors which matches the boundary conditions at the surfaces of the conductors. The current-carrying conductors are thus supplanted by phantom currents flowing in the medium itself. Within actual conductors the current density is related to the electric intensity by Ohm's Law, but for nonferromagnetic metals the permeability and permittivity are approximately equal to those of free space.[4] Therefore, in all practical cases it is an extremely good approximation to identify ι with the actual current distribution in the conductors.

Assume then that the conductors are indistinguishable from the dielectric medium, except that within them Ohm's Law applies.

$$\iota = \sigma_c E \tag{9}$$

where σ_c is the conductivity of the conductors. Then from (2) and (6) the first relationship between ι and ϕ is obtained.

$$\nabla\phi = -\frac{\iota}{\sigma_c} - \frac{\mu}{4\pi}\int_{\Omega} \frac{1}{r}\,\frac{\partial}{\partial t}\,\iota\left(t - \frac{r}{c}\right) d\Omega. \tag{10}$$

The second relationship is obtained by eliminating ρ between the time derivative of (7) and the equation of continuity of charge,

$$\nabla\cdot\iota = -\frac{\partial\rho}{\partial t}\,. \tag{11}$$

The result is

$$\frac{\partial\phi}{\partial t} = -\frac{1}{\pi 4\epsilon}\int_{\Omega} \frac{1}{r}\,\nabla\cdot\iota\left(t - \frac{r}{c}\right) d\Omega. \tag{12}$$

For points in the medium displaced by the conductors, (10) and (12) comprise a determinant set of simultaneous equations in ι and ϕ, which will be called the "complete circuit equations." Like the ordinary transmission line equations, these equations are *circuital* relationships, in that they can be solved for the current and potential at points in the conducting wire without the need for first determining expressions for the fields external to the wire. Eqs. (10) and (12) are *complete* in the sense that they take into account both wave retardation (radiation) and inductance and capacitance distribution. Therefore, a particular solution of these equations which fits the given boundary conditions is an accurate description of actual propagation along a system of conductors, especially if those conductors are extremely thin. For a system consisting entirely of spaced thin wires, the correspondence is extremely close at all wavelengths which are large compared with the largest wire diameter, regardless of the physical properties of the wire material. Thus, in most practical cases, where the wire diameter is much smaller than 3 mm, solutions of (10) and (12) are applicable up to at least 100,000 megacycles. Since the permeability and permittivity of actual nonferromagnetic metal wires closely approximate the free-space values, the validity of the complete circuit equations should extend even to much higher frequencies.

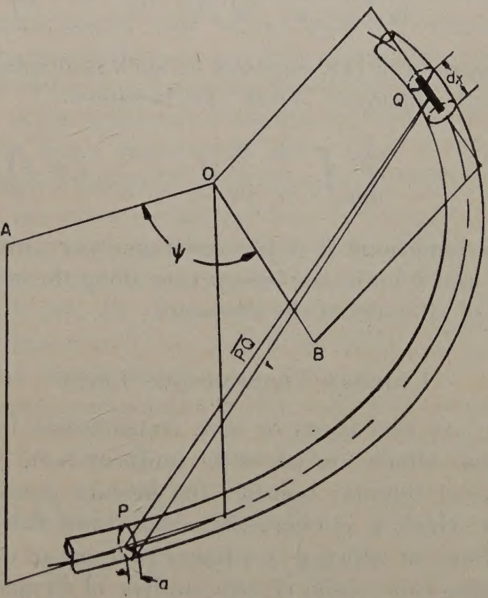

Fig. 1—Definitions of retardation distance r and angle ψ.

If the wire diameter is small compared with the free-space wavelength and if the distance between any two turns of wire is large compared with the wire diameter, then it is also a very good approximation to represent the current flow by means of filamentary currents flowing along the axes of the wires, and to assume that planes normal to the axis of each wire cut that wire in equipotential circles. The only component of $\nabla\phi$ which survives is then the one parallel to the wire axis, namely $\partial\phi/\partial s$, and the divergence of the current is simply $\partial_\iota/\partial s$. Therefore, the volume integrals in the complete circuit equations can both be replaced with scalar line integrals along the current path, as shown in Fig. 1.

---

[4] Stratton, *op. cit.*, chap. 5, p. 326.

The potential is evaluated at a point on the circumference of the wire at position P, a distance s along the wire from an arbitrary origin $s=0$. The current element at Q, a distance x along the wire from P, or $s+x$ from the origin, is $i\,dx$, and the corresponding retardation distance is conveniently taken to be

$$r = (a^2 + \overline{PQ}^2)^{1/2} \tag{13}$$

where a is the wire radius. This choice leads to the proper distance $r=a$ in the limit as x approaches zero. If the radius of the wire were ignored, the integrands would approach infinity as x approaches zero, and the integrals would diverge.

To obtain the component of the vector integral in (10) in the direction of the gradient of the scalar potential at P, the integrand is multiplied by $\cos\psi$, where ψ is the angle formed by intersecting lines $\overline{OA}$ and $\overline{OB}$, parallel to the wire axis at P and at Q, respectively. The resulting scalar line integral is

$$\frac{\partial\phi(t,s)}{\partial s} = -Ri(t,s) - \frac{\mu}{4\pi}\int_L \frac{\cos\psi}{r}\frac{\partial}{\partial t}i\left(t-\frac{r}{c},\, s+x\right)dx. \tag{14}$$

The integrand of (12) requires no such multiplier, since it is a scalar quantity. Thus, (12) becomes

$$\frac{\partial\phi(t,s)}{\partial t} = -\frac{1}{4\pi\epsilon}\int_L \frac{1}{r}\frac{\partial}{\partial s}i\left(t-\frac{r}{c},\, s+x\right)dx. \tag{15}$$

In these equations R is the resistance per unit length of wire, and L indicated integration along the combined lengths of all wires in the structure.

Uniform Transmission Lines

There are two types of wire transmission line configurations which are perfectly uniform (i.e., have no geometrical singular points): the infinite parallel-wire line, for which ψ is everywhere zero, and the infinite helical line, for which ψ is a linear function of distance. These lines can consist of any number of elements, but for a multi-element helical line to be perfectly uniform, the various helixes must be concentric, wound in the same direction, and have the same pitch. This paper will be concerned mainly with two-element lossless lines, although the results will also be used to calculate the performance of single-wire lossless lines.

The complete circuit equations for the first wire of a uniform two-wire lossless line can be written as

$$\frac{\partial\phi_1(t,s)}{\partial s} = -\frac{\mu K_1^2}{4\pi}\int_{-\infty}^{\infty}\frac{\cos\psi_{11}}{r_{11}}\frac{\partial}{\partial t}i_1\left(t-\frac{r_{11}}{c},\, s+x\right)dx$$
$$-\frac{\mu K_1K_2}{4\pi}\int_{-\infty}^{\infty}\frac{\cos\psi_{12}}{r_{12}}\frac{\partial}{\partial t}i_2\left(t-\frac{r_{12}}{c},\, s+x\right)dx \tag{16}$$

$$\frac{\partial\phi_1(t,s)}{\partial t} = -\frac{1}{4\pi\epsilon}\int_{-\infty}^{\infty}\frac{1}{r_{11}}\frac{\partial}{\partial s}i_1\left(t-\frac{r_{11}}{c},\, s+x\right)dx$$
$$-\frac{1}{4\pi\epsilon}\int_{-\infty}^{\infty}\frac{1}{r_{12}}\frac{\partial}{\partial s}i_2\left(t-\frac{r_{12}}{c},\, s+x\right)dx, \tag{17}$$

where s and x are measured along the axis of the line rather than along the axis of the wire itself, and K_1 and K_2 are the lengths of wires 1 and 2 per unit axial length. Similar equations can be written for line 2 by interchanging the subscripts 1 and 2.

If line 1 consists of two parallel wires of radius a spaced a distance d apart, the parameters are as follows:

$$K_1 = K_2 = 1, \qquad \psi_{11} = \psi_{12} = \psi_{21} = \psi_{22} = 0$$
$$r_{11} = r_{22} = (a^2 + x^2)^{1/2}, \tag{18}$$
$$r_{12} = r_{21} = (a^2 + d^2 + x^2)^{1/2}.$$

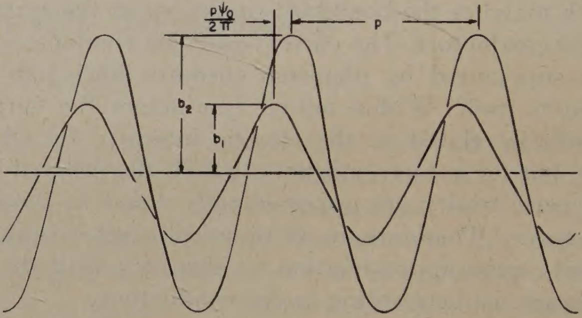

Fig. 2—The double helix.

For a double helix, such as shown in Fig. 2, the following parameters apply:

$$K_1 = \sqrt{1+\left(\frac{2\pi b_1}{p}\right)^2}, \qquad K_2 = \sqrt{1+\left(\frac{2\pi b_2}{p}\right)^2},$$
$$\psi_{11} = \psi_{22} = \frac{2\pi}{p}x$$
$$\psi_{12} = \frac{2\pi x}{p} - \psi_0, \qquad \psi_{21} = \frac{2\pi x}{p} + \psi_0$$
$$r_{11} = \sqrt{a^2 + 2b_1^2\left(1-\cos\frac{2\pi x}{p}\right) + x^2}$$
$$r_{22} = \sqrt{a^2 + 2b_2^2\left(1-\cos\frac{2\pi x}{p}\right) + x^2}$$
$$r_{12} = \sqrt{b_1^2 + b_2^2 - 2b_1b_2\cos\left(\frac{2\pi x}{p} - \psi_0\right) + x^2}$$
$$r_{21} = \sqrt{b_1^2 + b_2^2 - 2b_1b_2\cos\left(\frac{2\pi x}{p} + \psi_0\right) + x^2}. \tag{19}$$

If ι and ϕ vary sinusoidally with time, particular solutions of the complete circuit equations representing forward-wave propagation can be written in the form

$$i_1 = I_1 e^{j(\omega t - \beta s)}, \qquad i_2 = I_2 e^{j(\omega t - \beta s)} \tag{20}$$

$$\phi_1 = \Phi_1 e^{j(\omega t - \beta s)}, \qquad \phi_2 = \Phi_2 e^{j(\omega t - \beta s)}. \tag{21}$$

When these quantities are substituted back into the differential equations, the resulting expressions are four homogeneous linear equations in the four current and potential coefficients I_1, I_2, Φ_1, and Φ_2.

$$\beta\Phi_1 = \omega L_{11} I_1 + \omega L_{12} I_2 \tag{22}$$

$$\beta\Phi_2 = \omega L_{21} I_1 + \omega L_{22} I_2 \tag{23}$$

$$\omega\Phi_1 = \beta S_{11} I_1 + \beta S_{12} I_2 \tag{24}$$

$$\omega\Phi_2 = \beta S_{21} I_1 + \beta S_{22} I_2 \tag{25}$$

where the L's and S's represent the following integrals:

$$L_{mn} = \frac{\mu K_m K_n}{4\pi} \int_{-\infty}^{\infty} \frac{\cos \psi_{mn}}{r_{mn}} e^{-j(\omega/c) r_{mn}} e^{-j\beta x} dx \tag{26}$$

$$S_{mn} = \frac{1}{4\pi\epsilon} \int_{-\infty}^{\infty} \frac{1}{r_{mn}} e^{-j(\omega/c) r_{mn}} e^{-j\beta x} dx. \tag{27}$$

In order to obtain values of I_1, I_2, Φ_1, and Φ_2 that satisfy (22)–(25) and are not all zero, it is necessary that the determinant of these four equations be identically zero. This fourth-order determinant can be reduced to the second order by first eliminating Φ_1 between (22) and (24) and Φ_2 between (23) and (25). The determinant of the resulting two equations in I_1 and I_2 is then

$$\begin{vmatrix} (\beta^2 S_{11} - \omega^2 L_{11}) & (\beta^2 S_{12} - \omega^2 L_{12}) \\ (\beta^2 S_{21} - \omega^2 L_{21}) & (\beta^2 S_{22} - \omega^2 L_{22}) \end{vmatrix} = 0. \tag{28}$$

The values of β which satisfy this equation are the phase coefficients of the various modes of propagation of the two-wire line.

The phase coefficient for lossless parallel-wire lines is readily obtained. By substituting for the K's, ψ's, and r's in the right member of (26) and (27) their values given in (18), it is seen that $L_{mn} = S_{mn}/c^2$. Thus, the only solution of (28) for thin-wire lossless parallel lines is $\beta = \pm\omega/c$.

Determining the phase coefficients for helical lines is considerably more complicated. In the first place, β is not given explicitly; the expansion of (28) is a quadratic in β^2, and the coefficients of this quadratic themselves depend upon β, owing to the term $e^{-j\beta x}$, which appears in (26) and (27). In general, there are as many major modes as there are helixes, and additional minor modes also can occur as a consequence of the fact that L_{mn} and S_{mn} are functions of β. A second complication arises from the fact that these functions do not converge for all values of the parameter β. This difficulty is treated in the following section.

CONVERGENCE OF THE WAVE PARAMETERS

It will be convenient to write L_{mn} and S_{mn} as the Fourier transforms of

$$M_{mn}(x) = \frac{\mu K_m K_n \cos \psi_{mn}}{4\pi r_{mn}} e^{-j(\omega/c) r_{mn}} \tag{29}$$

$$T_{mn}(x) = \frac{1}{4\pi\epsilon r_{mn}} e^{-j(\omega/c) r_{mn}}. \tag{30}$$

Thus, (26) and (27) can be written as

$$L_{mn}(\beta) = \int_{-\infty}^{\infty} M_{mn}(x) e^{-j\beta x} dx \tag{31}$$

$$S_{mn}(\beta) = \int_{-\infty}^{\infty} T_{mn}(x) e^{-j\beta x} dx \tag{32}$$

and it is seen that x and β are the analogs of t and ω, respectively, the variables commonly used in connection with the Fourier integral to describe functions of time.

M_{mn} and T_{mn} will be called the self- and mutual "inductance distribution functions" and "elastance distribution functions," respectively; and their Fourier transforms, L_{mn} and S_{mn}, will be called the self- and mutual "wave inductances" and "wave elastances," respectively. These wave parameters are generalizations of the distributed inductances and elastances (reciprocal capacitances) of conventional transmission line theory. However, the wave parameters differ from previous distributed parameters in three respects: (1) they are functions of the phase coefficient β as well as of frequency; (2) the total number of wave inductances and elastances needed to describe an N-wire line is $2N^2$ instead of $2(N-1)^2$; and (3) the wave parameters are not necessarily symmetrical; i.e., L_{mn} is not identically L_{mn} and S_{mn} is not identically S_{nm}.

However, examination of (18) and (19) reveals that

$$M_{mn}(x), \; M_{nm}(-x); \quad T_{mn}(x), \; T_{nm}(-x) \tag{33}$$

from which it is readily shown that

$$L_{mn}(\beta), \; L_{nm}(-\beta); \quad S_{mn}(\beta), \; S_{nm}(-\beta). \tag{34}$$

Thus, it can be seen that if $+\beta$ is a root of the characteristic equation (28), then so is, $-\beta$, confirming the fact that uniform transmission lines, in common with all other iterated passive networks, are bilateral.

For the wave inductances and elastances to have meaning, it is necessary that the integrals they represent converge. Since the integrands are bounded functions of x, their convergence depends entirely upon the behavior of the integrands for large x. Each of the T's has an asymptote of the form

$$T(x) = \frac{e^{-j(\omega/c)\sqrt{A^2+x^2}}}{4\pi\epsilon\sqrt{A^2 + x^2}} \cdot \tag{35}$$

We will now consider the Fourier transform of this function, first for real values of β and then for complex values.

For real values of β the Fourier transform of $T(x)$ is[5]

$$S(\beta) = \frac{1}{2\pi\epsilon} K_0\left(A\sqrt{\beta^2 - \left(\frac{\omega}{c}\right)^2}\right) \qquad (36)$$

which exists for all real β, except $\beta = \pm\omega/c$, that is, except for zero arguments of the modified Bessel function K_0. Using the small-argument asymptote of this function[6]

$$S(\beta) \approx -\frac{1}{2\pi\epsilon}\left\{\frac{1}{2}\ln\left[\beta^2-\left(\frac{\omega}{c}\right)^2\right]+\ln A+C-\ln 2\right\} \qquad (37)$$

where C is Euler's constant $0.5772157 \cdots$. Thus, it is seen that the wave elastances of all perfectly uniform lines (parallel-wire and helical) have logarithmic singularities at $\beta = \pm\omega/c$.

Likewise, for parallel-wire lines the wave inductances have logarithmic singularities at $\beta = \pm\omega/c$. However, for helical lines each of the M's contains an additional periodic factor, $\cos\psi_{mn}$, of periodicity $2\pi/p$, where p is the helix pitch; consequently, the singularities of the wave inductances of helical lines are displaced from those of the wave elastances by the amounts $\pm 2\pi/p$. These singular points are

$$\beta_1 = \frac{2\pi}{p} + \frac{\omega}{c}, \qquad \beta_3 = -\frac{2\pi}{p} + \frac{\omega}{c}$$

$$\beta_2 = \frac{2\pi}{p} - \frac{\omega}{c}, \qquad \beta_4 = -\frac{2\pi}{p} - \frac{\omega}{c}.$$

As a consequence of these singularities of the wave inductances and elastances, the scalar potential diverges for the singular values of β. This in itself does not prevent the propagation of waves having these phase coefficients, because such waves are invariably excited by means of driving voltages which are *differences* of potential. These differences of potential can be determined by taking the Fourier integral of the difference between two distribution functions, and such Fourier integrals converge for the singular values of β, owing to a mutual cancellation of the logarithmic singularities. Therefore, the potential differences which occur in the neighborhood of a uniform line are convergent for all real values of β.

For complex values of β, such as $\beta - j\alpha$, the Fourier integrand contains the exponential factor $e^{-\alpha x}$. This factor prevents the integrand from approaching zero as x approaches $-\infty$. Likewise, it prevents the difference between two such integrands from approaching zero, unless the two integrands are identical. Therefore, the infinite Fourier integrals involved in determining scalar potential and differences in scalar potential all necessarily diverge, unless $\alpha = 0$. From this it is seen that lossy waves cannot exist on a transmission line which is "perfectly uniform" in the sense that the line is without geometric singularities.

This restricts the domain of variation of β for which solutions can be obtained to points on the real-β axis. However, the presence of the retardation factor $e^{-j\omega r_{mn}/c}$ in (29) and (30) makes it possible for the wave inductances and elastances corresponding to real values of β to be complex. It will be shown in the following section that if β is real and satisfies

$$\left|\beta - \frac{2\pi k}{p}\right| > \left|\frac{\omega}{c}\right| \qquad (38)$$

for all integers k, including zero, then all the wave parameters are real, except the mutual inductances and elastances of unsymmetrical double helixes (viz., Fig. 2 for ψ_0 not zero). Furthermore, it is found that to each value of β satisfying (38) there correspond one or more frequencies for which that value is a root of the characteristic determinant, (28). The unsymmetrical double helix is no exception to this, because L_{mn} and S_{mn} happen to be conjugates of L_{nm} and S_{nm}, respectively, and as a result the imaginary part of the characteristic determinant is identically zero for all real values of β that satisfy (38).

For real values of β that do not satisfy (38), all the wave parameters are complex and not conjugate. It is extremely unlikely that these complex values would lead to real-β roots of the characteristic determinant, except perhaps in isolated instances; that is, one would expect complex values of L_{mn} and S_{mn} to be associated with complex-β roots of the characteristic determinant, but L_{mn} and S_{mn} for complex values of β do not exist, because the integrals which they represent diverge. Consequently, exponential propagation occurs only for real values of β within the intervals defined by (38), except perhaps for isolated points outside those intervals, where (28) might be satisfied coincidentally by real values of β and complex values of the wave parameters.

An explanation of the physical significance of the prohibited ranges of β will not be attempted here. However, some pertinent facts upon which an explanation in terms of outward radiation or excessive velocity of energy propagation might be based are contained in (38). For $k=0$ the prohibited range is

$$|\beta| < \left|\frac{\omega}{c}\right|; \quad \text{or} \quad v > c. \qquad (39)$$

That is, for propagation to occur, the axial phase velocity must be less than the velocity of light. For the other ranges let the wavelength of propagation be λ and the wavelength of a plane wave in the medium be λ_0. Then

---

[5] G. A. Campbell and R. M. Foster, "Fourier Integrals for Practical Applications," D. Van Nostrand Company, Inc., New York, N. Y., pair no. 917, p. 125; 1942.

[6] S. A. Schelkunoff, "Electromagnetic Waves," D. Van Nostrand Company, Inc., New York, N. Y., chap. 3, p. 51; 1948.

$$\beta = \frac{2\pi}{\lambda}, \qquad \frac{\omega}{c} = \frac{2\pi}{\lambda_0}. \tag{40}$$

Upon substituting for β and ω/c in (38) and rearranging, it is found that the following prohibited ranges of propagation wavelength correspond to the prohibited ranges of β:

$$\frac{p/k}{1 + \dfrac{p}{k\lambda_0}} < \lambda < \frac{p/k}{1 - \dfrac{p}{k\lambda_0}}. \tag{41}$$

These are small neighborhoods of the values for which the helix pitch p is an integral number of wavelengths.

Although certain ranges of β are prohibited, this does not necessarily mean that there are also gaps in the range of frequencies over which propagation can occur. In fact the plots of phase velocity given later reveal that propagation in one mode or another occurs at all frequencies. There are certain modes for which the plot of phase velocity versus frequency terminates in a point; but it also happens that some of these plots double back on themselves, giving rise to extrema of frequency and multivaluedness within a single major mode. Expressed differently, the variation of the L's and S's with β generate additional minor modes; the domains of variation of frequency for all of the major and minor modes form a set of overlapping line segments which covers the entire frequency spectrum.

However, this is not to say that an actual helix, having large but finite maximum-Q values, will propagate effectively at all frequencies. The model being considered here is an infinite-Q structure. For an actual helix to be accurately represented by such a model, the wave inductance must be very large compared with the wire resistance per unit length. For certain ranges of the phase coefficient β the wave inductance is very low, and consequently the propagation will be very lossy in the mode segments associated with those ranges of β.

HELIX WAVE INDUCTANCES AND ELASTANCES

To obtain expressions for L_{mn} and S_{mn} suitable for numerical calculations, a more compact notation will be used; the subscripts will be dropped, and the retardation distance r_{mn} will be represented by

$$r = \sqrt{A^2 - B^2 \cos\psi + x^2} \tag{42}$$

where the numbers A and B assume different values for r_{11}, r_{12}, etc. [cf. (19)], and

$$\psi = \frac{2\pi x}{p} + \psi_1, \tag{43}$$

where ψ_1 is $-\psi_0$ for L_{12} and S_{12}, $+\psi_0$ for L_{21} and S_{21}, and zero for L_{11}, and L_{22}, S_{11}, and S_{22}; it is zero for all the wave parameters of a symmetrical double helix, for which $\psi_0 = 0$. The product K_mK_n will be simply K^2. The distribution functions of the double helix are then

$$M(x) = \frac{\mu K^2}{4\pi} \frac{e^{-j(\omega/c)r}}{r} \cos\psi \tag{44}$$

$$T(x) = \frac{1}{4\pi\epsilon} \frac{e^{-j(\omega/c)r}}{r}. \tag{45}$$

Since $M(x)$ and $T(x)$ are even periodic functions of ψ, regarded as an independent variable, they can be expanded as Fourier cosine series.

$$\begin{aligned} M(x, \psi) &= m_0(x) + 2m_1(x)\cos\psi \\ &\quad + 2m_2(x)\cos 2\psi + \cdots \end{aligned} \tag{46}$$

$$\begin{aligned} T(x, \psi) &= t_0(x) + 2t_1(x)\cos\psi \\ &\quad + 2t_2(x)\cos 2\psi + \cdots \end{aligned} \tag{47}$$

where

$$m_k(x) = \frac{1}{2\pi}\int_0^{2\pi} M(x, \psi)\cos k\psi d\psi \tag{48}$$

$$t_k(x) = \frac{1}{2\pi}\int_0^{2\pi} T(x, \psi)\cos k\psi d\psi. \tag{49}$$

Using

$$2\cos k\psi = e^{jk\psi_1}e^{j(2\pi k/p)x} + e^{-jk\psi_1}e^{-j(2\pi k/p)x} \tag{50}$$

the Fourier transforms of (46) and (47) are found to be

$$\begin{aligned} L(\beta) &= l_0(\beta) + e^{j\psi_1}l_1\left(\beta - \frac{2\pi}{p}\right) + e^{-j\psi_1}l_1\left(\beta + \frac{2\pi}{p}\right) \\ &\quad + e^{j2\psi_1}l_2\left(\beta - \frac{4\pi}{p}\right) + e^{-j2\psi_1}l_2\left(\beta + \frac{4\pi}{p}\right) \\ &\quad + \cdots \end{aligned} \tag{51}$$

$$\begin{aligned} S(\beta) &= s_0(\beta) + e^{j\psi_1}s_1\left(\beta - \frac{2\pi}{p}\right) + e^{-j\psi_1}s_1\left(\beta + \frac{2\pi}{p}\right) \\ &\quad + e^{j2\psi_1}s_2\left(\beta - \frac{4\pi}{p}\right) + e^{-j2\psi_1}s_2\left(\beta + \frac{4\pi}{p}\right) \\ &\quad + \cdots \end{aligned} \tag{52}$$

where

$$l_k(\beta) = \int_{-\infty}^{\infty} m_k(x)e^{-j\beta x}dx \tag{53}$$

$$s_k(\beta) = \int_{-\infty}^{\infty} t_k(x)e^{-j\beta x}dx \tag{54}$$

$m_k(x)$, $t_k(x)$, $l_k(\beta)$, and $s_k(\beta)$ will be called the partial inductance distribution function, partial elastance distribution function, partial wave inductance, and partial wave elastance, respectively, all of order k. Upon substituting from (44), (45), (48), and (49), it is seen that

$$l_k(\beta) = \frac{\mu K^2}{8\pi^2}\int_{-\infty}^{\infty}\int_0^{2\pi}\frac{e^{-j(\omega/c)r}}{r}\cos\psi\cos k\psi e^{j\beta x}d\psi dx \quad (55)$$

$$s_k(\beta) = \frac{1}{8\pi^2\epsilon}\int_{-\infty}^{\infty}\int_0^{2\pi}\frac{e^{-j(\omega/c)r}}{r}\cos k\psi e^{j\beta x}d\psi dx. \quad (56)$$

The order of integration of these double integrals can be reversed, provided that for either order of integration the first integral is uniformly convergent throughout the range of the second integration.[7] Since the integrands are continuous, the finite ψ integrals are uniformly convergent with respect to x. The infinite x integrals (Fourier transforms) are the same functions used earlier in this paper [cf. (35) and (36)].

$$\int_{-\infty}^{\infty}\frac{e^{-j(\omega/c)\sqrt{A^2-A^2\cos\psi+x^2}}}{\sqrt{A^2-B^2\cos\psi+x^2}}e^{-j\beta x}dx$$
$$= 2K_0\left(\sqrt{A^2-B^2\cos\psi}\sqrt{\beta^2-\left(\frac{\omega}{c}\right)^2}\right). \quad (57)$$

They are uniformly convergent with respect to ψ, provided $\beta^2 \neq (\omega/c)^2$. Thus, it is permissible to reverse the order of integration in (55) and (56) and the resulting integrals are

$$l_k(\beta) = \frac{1}{2\pi}\int_0^{2\pi}\frac{\mu K^2}{2\pi}K_0\left(\sqrt{A^2-B^2\cos\psi}\sqrt{\beta^2-\left(\frac{\omega}{c}\right)^2}\right)\cos\psi d\psi \quad (58)$$

$$s_k(\beta) = \frac{1}{2\pi}\int_0^{2\pi}\frac{1}{2\pi\epsilon}K_0\left(\sqrt{A^2-B^2\cos\psi}\sqrt{\beta^2-\left(\frac{\omega}{c}\right)^2}\right)d\psi. \quad (59)$$

Thus, the wave inductances and elastances are obtained as functions of β by first determining the quantities $l_0(\beta)$, $l_1(\beta)$, $l_2(\beta)$, $\cdots$ and $s_0(\beta)$, $s_1(\beta)$, $s_2(\beta)$, $\cdots$, which turn out to be Fourier series coefficients of quantities involving β in the radical $[\beta^2-(\omega/c)^2]^{1/2}$. The arguments of l_k and s_k are then shifted by the amounts $\pm 2\pi k/p$, and the corresponding values of the quantities l_k and s_k are entered into the sums in (51) and (52).

Since β appears only in the radical, it is convenient to give that radical a special name and symbol. It will be called the *phase parameter* δ, given by

$$\delta = [\beta^2 - (\omega/c)^2]^{1/2}. \quad (60)$$

Then the partial wave inductances and elastances, written as functions of δ, become

$$l_k(\delta) = \frac{\mu K^2}{4\pi^2}\int_0^{2\pi}K_0(\delta\sqrt{A^2-B^2\cos\psi})\cos\psi\cos k\psi d\psi \quad (61)$$

$$s_k(\delta) = \frac{1}{4\pi^2\epsilon}\int_0^{2\pi}K_0(\delta\sqrt{A^2-B^2\cos\psi})\cos k\psi d\psi, \quad (62)$$

and the total wave inductance and elastance become

$$L(\beta) = l_0(\delta_0) + l_1(\delta_1) + l_1(\delta_{-1}) + l_2(\delta_2) + l_2(\delta_{-2}) + \cdots \quad (63)$$

$$S(\beta) = s_0(\delta_0) + s_1(\delta_1) + s_1(\delta_{-1}) + s_2(\delta_2) + s_2(\delta_{-2}) + \cdots \quad (64)$$

where

$$\delta_k = \left[\left(\beta - \frac{2\pi k}{p}\right)^2 - \left(\frac{\omega}{c}\right)^2\right]^{1/2}. \quad (65)$$

The modified Bessel function K_0, appearing in (61) and (62) is real for positive real arguments and complex for imaginary arguments. Therefore, it follows from (51), (52), (58), and (59) that all of the l's and s's involved in the expressions for $L(\beta)$ and $S(\beta)$ will be real, provided that

$$\left|\beta - \frac{2\pi k}{p}\right| > \left|\frac{\omega}{c}\right| \quad (66)$$

for all integers k (positive, negative, and zero). It also follows from (51) and (52) that since ψ_1 is zero for L_{11}, L_{22}, S_{11}, and S_{22}, these wave parameters are *real* for values of satisfying (66); and since ψ_1 is $-\psi_0$ for L_{12} and S_{12} and $+\psi_0$ for L_{21} and S_{21}, the mutual wave parameters are *conjugate* for values of β satisfying (66).

Some calculated values of the partial wave inductances, elastances, and capacitances (inverse elastances) of single and double helixes are presented in graphical form in Figs. 3–5. For clarity the notation $L_{mn}(k=0)$, $L_{mn}(k=1)$, $\cdots$ $S_{mn}(k=0)$, $S_{mn}(k=1)$, $\cdots$ is used to represent the partial wave parameters l_0, l_1, $\cdots$ s_0, s_1, $\cdots$ corresponding to L_{mn} and S_{mn} of the double helix. A similar notation $L(k=0)$, $L(k=1)$, etc., is used for the single helix.

SEGREGATION OF PROPAGATION MODES ON BASIS OF WAVELENGTH

In helixes with sufficiently large ratios of circumference to pitch the calculated values of total wave inductance $L(\beta)$ and total wave elastance $S(\beta)$ display a peculiar "wavelength resonance" phenomenon. For example, when β is very small compared with $2\pi/p$, δ_0 is

---

[7] G. A. Gibson, "Advanced Calculus," Macmillan and Company, Ltd., London, Eng., chap. XIV, theorem I, p. 446; 1931.

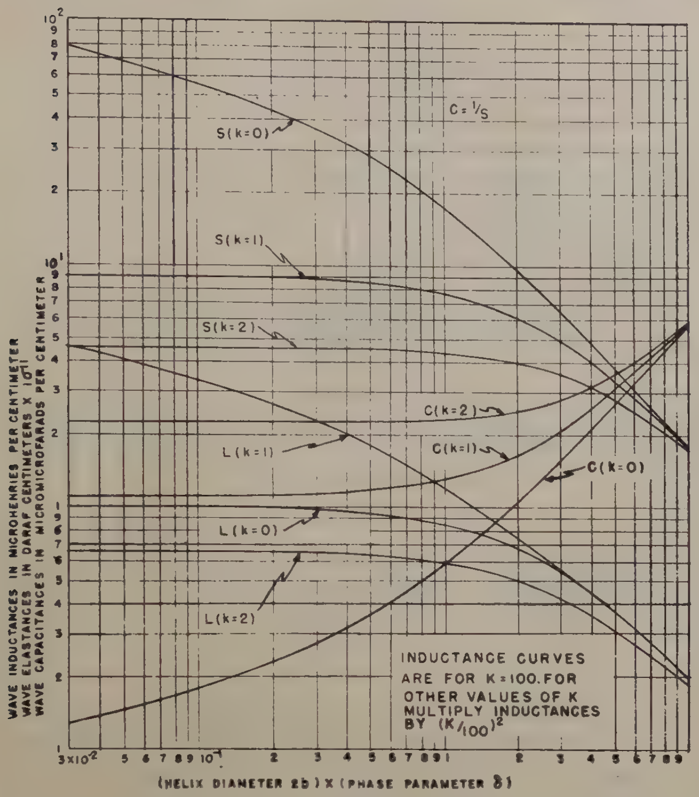

Fig. 3—Single-helix partial wave inductances, wave elastances, and wave capacitances (inverse wave elastances) of orders 0, 1, and 2 vs phase parameter.

small, and $l_0(\delta_0)$ and $S_0(\delta_0)$ are near their maximum values. On the other hand, for the same values of β the other δ's are large, and the other l's and s's are much smaller than their maximum values, so that for K_1 and K_2 both sufficiently large the calculated values of $L(\beta)$ and $S(\beta)$ are closely approximated by the first terms of (63) and (64).

$$L(\beta) \approx l_0(\delta_0) \qquad \left(|\beta| \ll \frac{2\pi}{p}\right) \qquad (67)$$

$$S(\beta) \approx s_0(\delta_0) \qquad \left(|\beta| \ll \frac{2\pi}{p}\right). \qquad (68)$$

Similarly, for β near $2\pi/p$,

$$L(\beta) \approx l_1(\delta_1)e^{j\psi_1} \qquad \left(\left|\beta - \frac{2\pi}{p}\right| \ll \frac{2\pi}{p}\right) \qquad (69)$$

$$S(\beta) \approx s_1(\delta_1)e^{j\psi_1} \qquad \left(\left|\beta - \frac{2\pi}{p}\right| \ll \frac{2\pi}{p}\right). \qquad (70)$$

The same is true to a smaller extent for $4\pi/p$: that is,

$$L(\beta) \approx l_2(\delta_2)e^{j2\psi_1} \qquad \left(\left|\beta - \frac{4\pi}{p}\right| \ll \frac{2\pi}{p}\right) \qquad (71)$$

$$S(\beta) \approx s_2(\delta_2)e^{j2\psi_1} \qquad \left(\left|\beta - \frac{4\pi}{p}\right| \ll \frac{2\pi}{p}\right). \qquad (72)$$

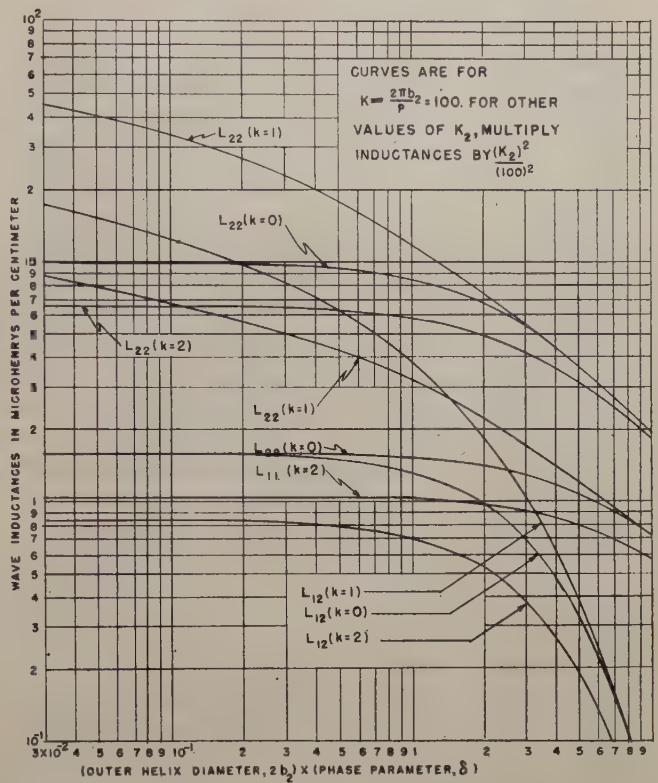

Fig. 4—Double-helix partial wave inductances of orders 0, 1, and 2 vs phase parameter ($b_1/b_2=0.4$).

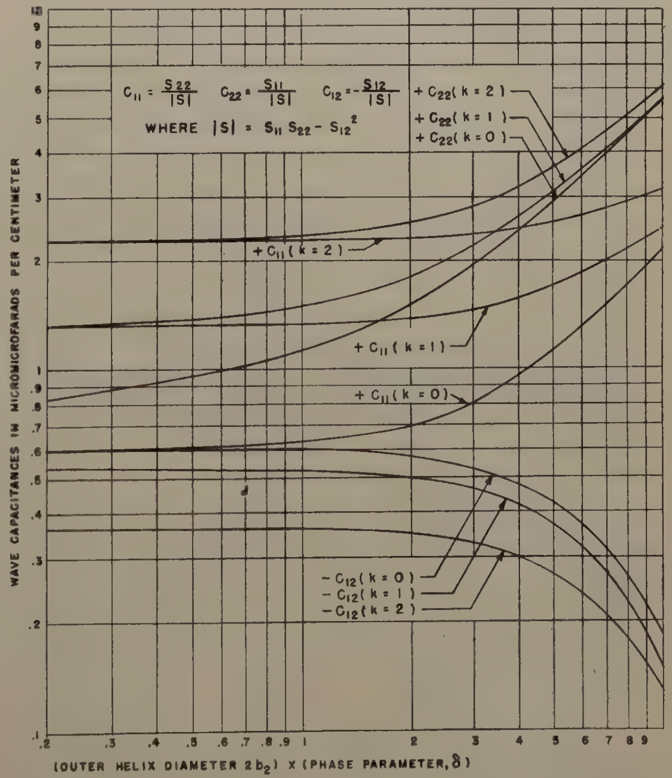

Fig. 5—Double-helix partial wave capacitances (inverse wave elastances) of orders 0, 1 and 2 vs phase parameter ($b_1/b_2=0.4$).

Utilizing these approximations greatly reduces the number of terms required in subsequent calculations, and more important, it enables the calculation of phase velocity *parametrically* in terms of one of the phase-parameter values δ_0, δ_1, δ_2, $\cdots$, the choice depending upon the range of wavelengths involved. For example, the phase velocity and frequency are both multiple-valued functions of δ_0 at wavelengths which are small compared with $2\pi/p$ (referred to as "video wavelengths" in the illustrations); at wavelengths near $2\pi/p$ (first-resonance wavelengths) the phase velocity and frequency are functions of δ_1, and near $4\pi/p$ (second-resonance wavelengths) they are functions of δ_2.

In performing the calculations for the partial wave inductances and elastances, given in the previous section, it is found that each of these quantities is practically independent of the wire radius a. On the other hand, it can be shown that the error incurred by using (67)–(72) has an upper bound which is largely affected by the choice of a, and most likely that error itself involves the wire radius as a principal variable. Certainly this is true in the limit as a approaches zero, for then the total wave inductance and total wave elastance diverge [cf. (13)]. Thus, the partial wave inductances and elastances individually display the attributes of "external impedance" and collectively display the attributes of "internal impedance."[8] The data of this paper will take cognizance of external impedance only, and for that reason the wire radius has been set equal to zero in the calculated partial wave parameters given above. Likewise, it does not enter into calculations given later in which the total wave parameters are each approximated by a single term from their expansions in terms of partial wave inductances and elastances.

By substituting ω/v for β the characteristic determinant (28) when expanded becomes a quadratic equation in v^2,

$$F_0 - F_1 v^2 + F_2 v^4 = 0 \tag{73}$$

where the quantity ω has been eliminated by factoring, and the coefficients are the following functions of L_{mn} and S_{mn}:

$$F_0 = S_{11}S_{22} - S_{12}S_{21} \tag{74}$$

$$F_1 = L_{11}S_{22} + L_{22}S_{11} - L_{12}S_{21} - L_{21}S_{12} \tag{75}$$

$$F_2 = L_{11}L_{22} - L_{12}L_{21}. \tag{76}$$

At wavelengths near $2\pi k/p$ substitutions of the following type can be made for each of the quantities L_{mn} and S_{mn}:

$$L(\beta) = l_k(\delta_k)e^{jk\psi_1} \tag{77}$$

$$S(\beta) = s_k(\delta_k)e^{jk\psi_1}. \tag{78}$$

Thus, for β near $2\pi k/p$ the quantities F_0, F_1, and F_2 are all explicit functions of δ_k, and v^2 can be determined in closed form as a function of δ_k by solving the quadratic equation, (73).

$$v^2 = \frac{F_1(\delta_k) \pm \sqrt{[F_1(\delta_k)]^2 - 4F_0(\delta_k)F_2(\delta_k)}}{2F_2(\delta_k)}. \tag{79}$$

Likewise, $f = \omega/2\pi$ can be determined in closed form by substituting $2\pi f/v$ for β in (63) and solving the resulting quadratic equation in f. The result is

$$f = \frac{1}{2\pi}\,\frac{v}{1-\left(\frac{v}{c}\right)^2}\left[\frac{2\pi k}{p} \pm \sqrt{\left(\frac{2\pi k v}{pc}\right)^2 + \left(1-\left(\frac{v}{c}\right)^2\right)\delta_k^2}\,\right]. \tag{80}$$

Plots of phase velocity versus frequency are made by choosing a sequence of values for the parameter δ_k and determining the corresponding values of f and v, which are then plotted against each other. For each value of f there are two values of v^2, owing to the ± sign in (79), which serves to identify the two major modes; the plus sign corresponds to the major mode associated with the smaller helix, and the minus sign corresponds to the major mode associated with the larger helix. Also, for each value of v there correspond two values of f, owing to the ± sign in (80), causing each of the major modes to be divided into two separate curves. The square root of v^2 has two values: $+v$, corresponding to forward-traveling waves, and $-v$, corresponding to backward-traveling waves. Thus, to each value of δ_k there correspond eight distinct points in the positive-frequency half of the f-v plane, except that for $k=0$ there are only four distinct points, owing to the fact that each of the eight roots coincides with one other root, thereby reducing the number of distinct roots to four.

In the case of the single helix, f is given by (80), as before, but the phase velocity squared is

$$v^2 = s_k(\delta_k)/l_k(\delta_k) \tag{81}$$

which does not contain a ± sign. Thus, the number of major modes is one, but this major mode subdivides into two curves, owing to the ± sign in (80).

Illustrative plots of phase velocity, impedance, and coupling coefficients are given in Figs. 6–13. Figs. 6–10 apply to single helixes having various ratios of circumference to pitch. Phase velocity is plotted as Kv/c, the ratio of the phase velocity, measured along the wire instead of axially, to the velocity of light. This ratio tends to unity for large phase parameters or at frequencies far removed from the "critical frequencies."

---

[8] Rano and Whinnery, *op. cit.*, chap. 6, pp. 207–208.

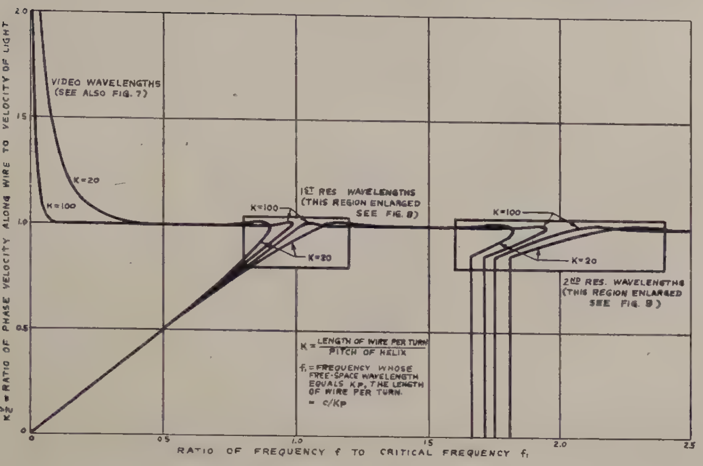

Fig. 6—Phase velocities of single helix vs frequency.

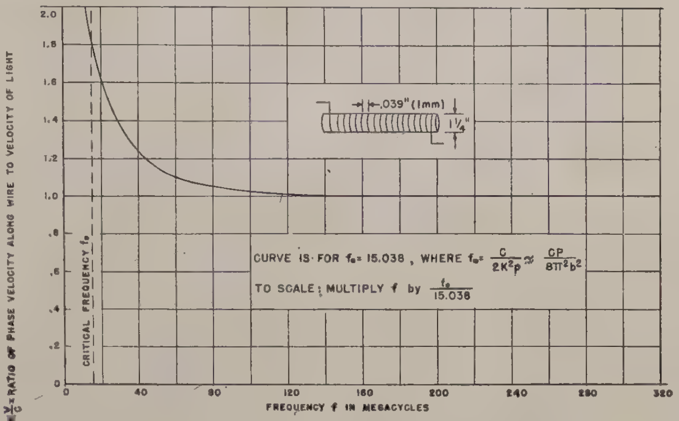

Fig. 7—Phase velocity of single helix vs frequency for video wavelengths.

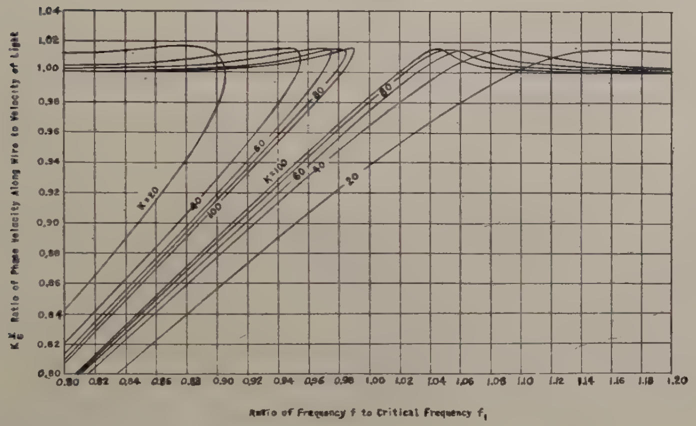

Fig. 8—Enlarged plot of phase velocity vs frequency for first-resonance wavelengths.

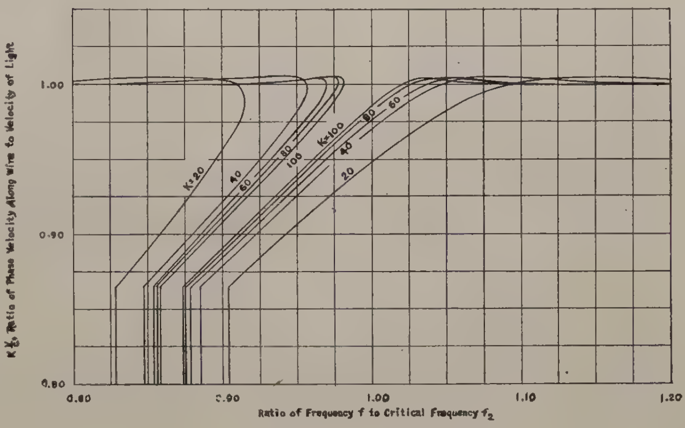

Fig. 9—Enlarged plot of phase velocity vs frequency for second-resonance wavelengths.

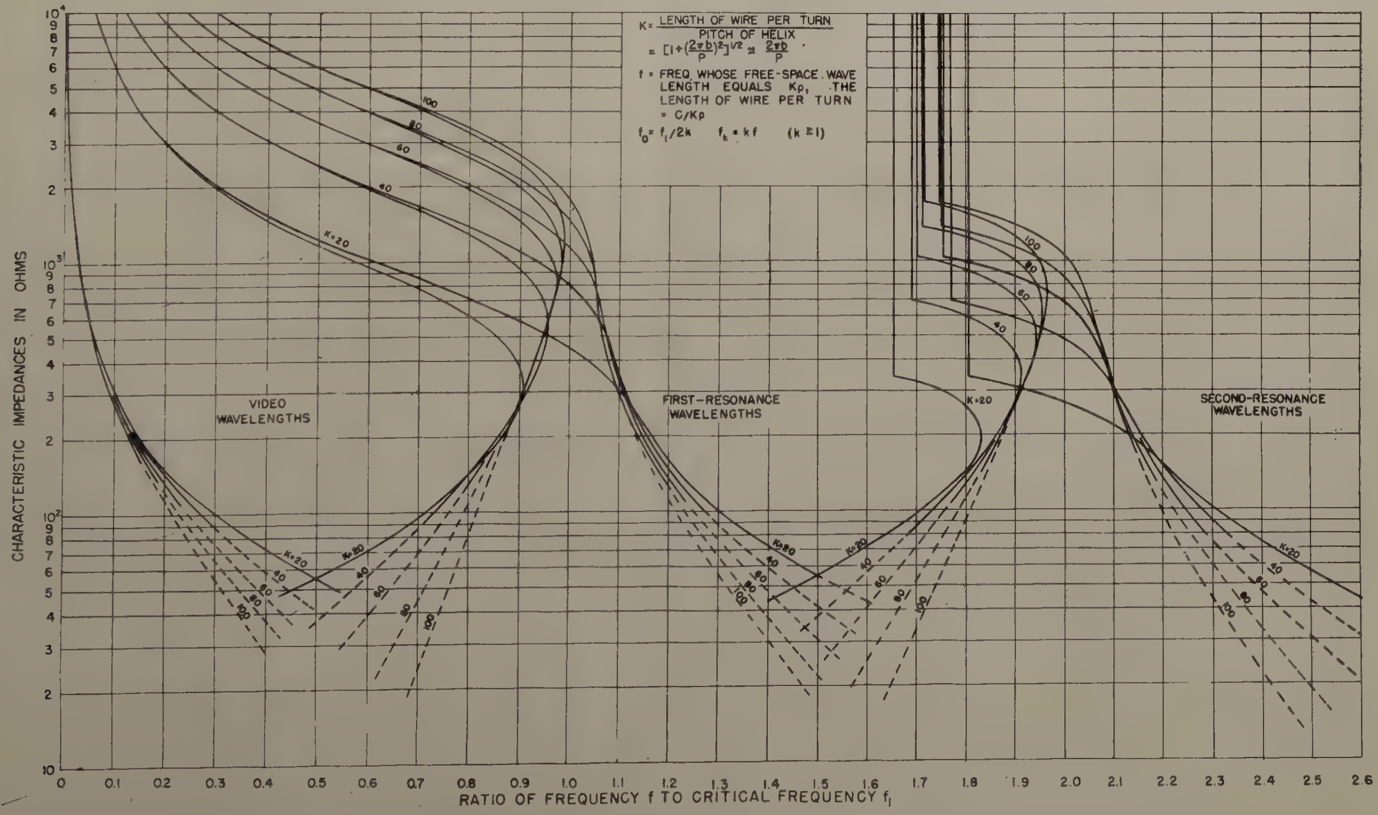

Fig. 10—Characteristic impedances of single helix vs frequency for video, first-resonance, and second-resonance wavelengths.

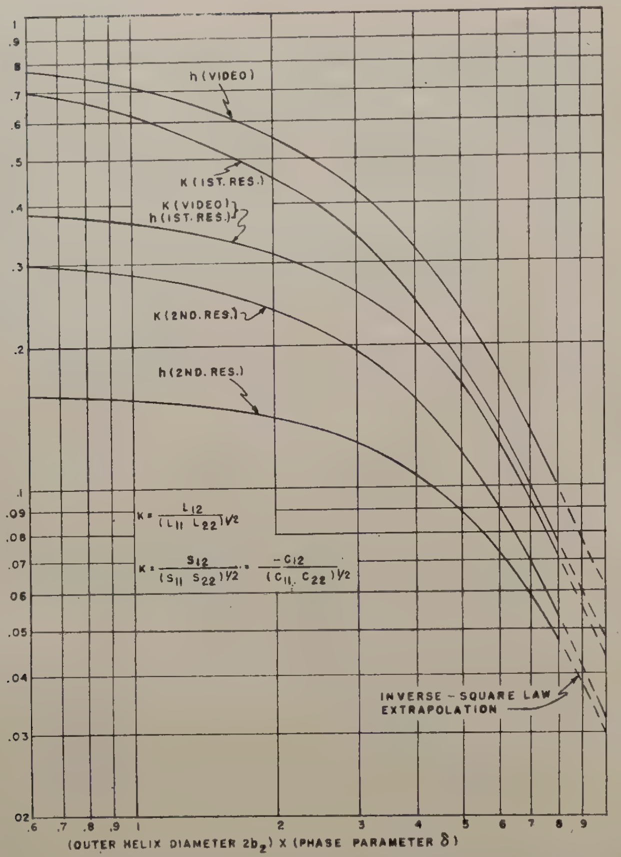

Fig. 11—Coupling coefficients of double helix vs phase parameter for video, first-resonance, and second-resonance wavelengths ($b_1/b_2=0.4$).

$$f_k = \frac{kc}{Kp} \qquad k = 1, 2, 3, \cdots \tag{82}$$

$$f_0 = \frac{f_1}{2K} = \frac{c}{2K^2p}. \tag{83}$$

This indicates a tendency for the propagated wave to follow the contour of the wire. The characteristic impedance of the single helix, shown in Fig. 10, is simply

$$Z_0 = \sqrt{l_k(\delta_k)s_k(\delta_k)}. \tag{84}$$

To aid in identifying the various curves in this figure some of them have been extended far beyond the last calculated points ($2b\delta=24$) by means of straight dotted lines. The curves related to second-resonance wavelengths terminate at points corresponding to $2b\delta_2=0$. This is indicated by vertical straight lines emanating from the terminal points.

Curves applying to double helixes having $b_1/b_2=0.4$ are given in Figs. 11–13. The electric and magnetic coupling coefficients, h and k, respectively, are plotted in Fig. 11 as functions of the phase parameter. These coefficients both approach zero as δ approaches infinity. Consequently, at frequencies far removed from all the critical frequencies of the individual helixes the double helix behaves like two separate single helixes, each propagating a wave which follows its respective contour. This is evidenced also by the plot of phase

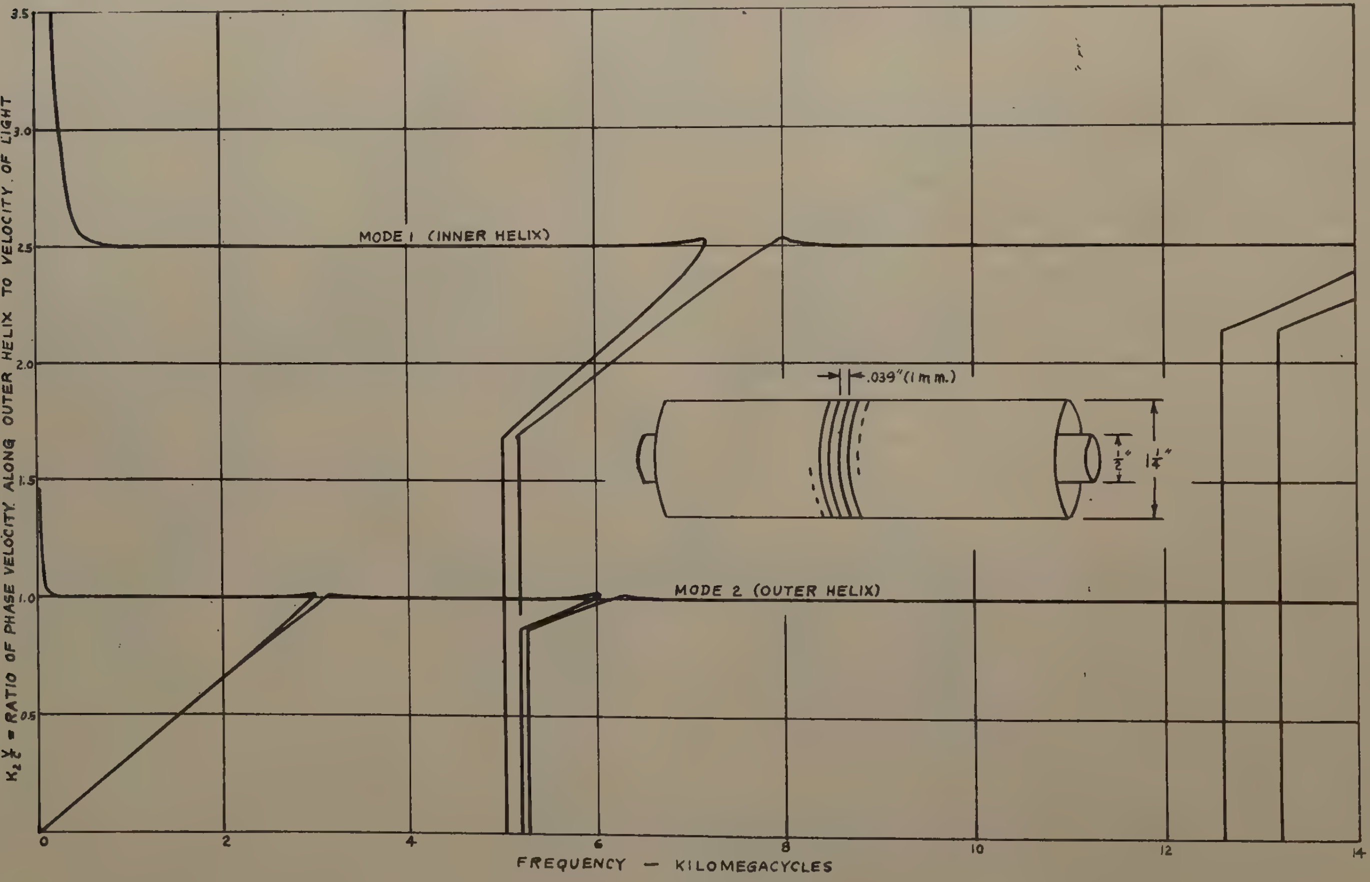

Fig. 12—Phase velocities of double helix vs frequency.

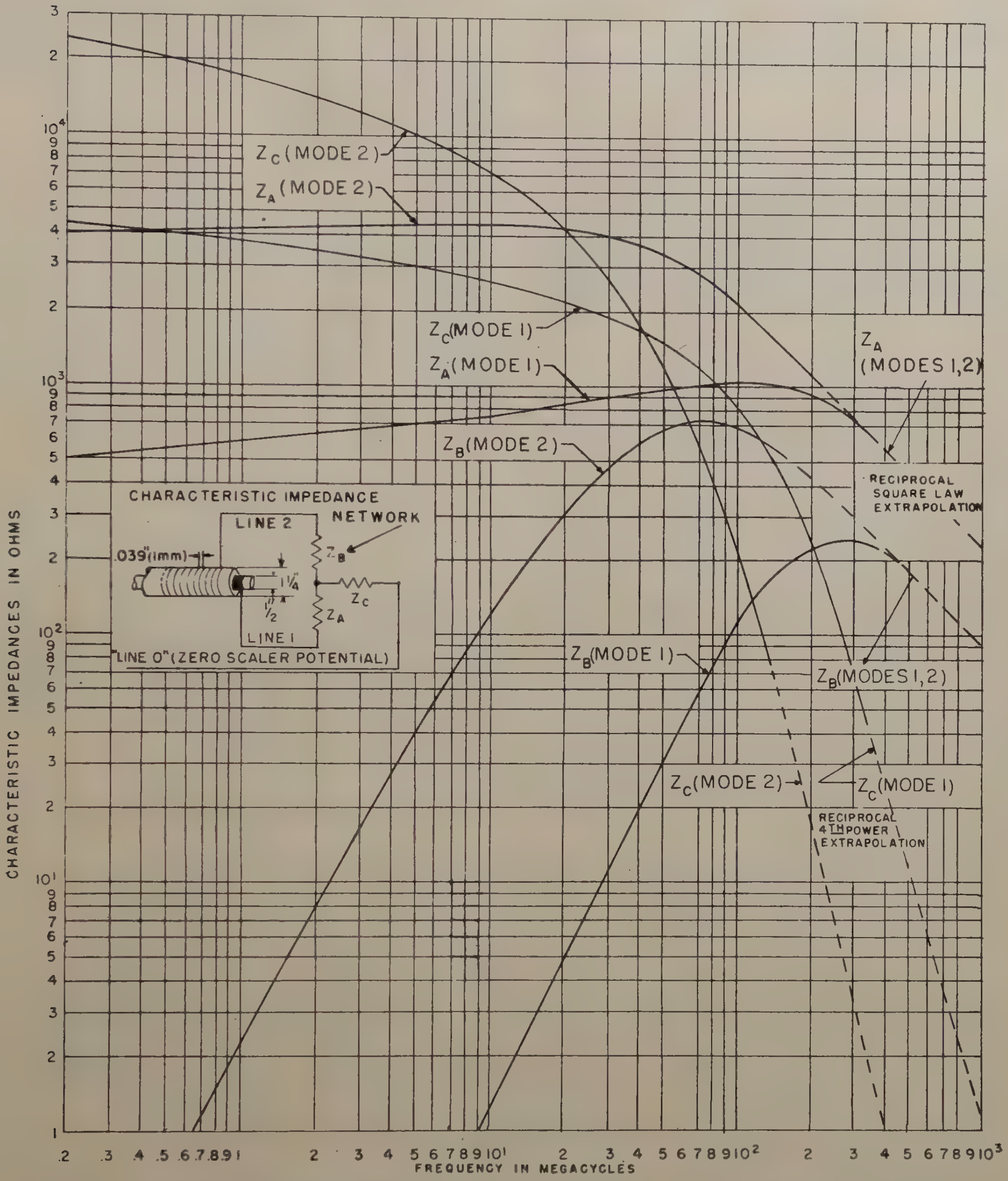

Fig. 13—Characteristic network component impedances of double helix vs frequency (video wavelengths).

velocity, measured along the *outer* helix, versus frequency, given in Fig. 12. For large values of the phase parameters δ_0, δ_1, and δ_2 that ratio approaches unity for the outer helix and 1/0.4 for the inner helix. The impedance of a double helix at video wavelengths is represented in Fig. 13 by three impedances, Z_A, Z_B, and Z_C, which, when connected as a T-section between the inner and outer helixes and a point of zero scalar potential, present the same impedance as does the double helix when it is propagating a single forward-traveling wave.

Acknowledgements

The author wishes to thank Dr. H. M. Von Foerster for his many helpful suggestions and criticisms throughout the course of this investigation, as well as Dr. E. C. Jordan for reviewing the manuscript.

Radiation from a Vertical Dipole over a Stratified Ground (Part II)*

J. R. WAIT† AND W. C. G. FRASER‡

Summary—**Further results are given for the problem of a vertical electric dipole situated over a horizontally stratified conductor. It is pointed out that under certain conditions the surface-wave field intensity for a stratified conducting ground is greater than the corresponding case for a perfectly conducting ground. Numerical values for the attenuation factor are also given.**

INTRODUCTION

IN A PREVIOUS paper (referred to as Part I),[1] the solution for a vertical electric dipole situated on a horizontally stratified ground was given. It was indicated that the final result could be put in a convenient form that was quite analogous to the well known result for the homogeneous ground by defining an effective propagation constant γ_e. It is the purpose of this paper to discuss the problem further and to outline a more general solution where several of the earlier restrictions have been relaxed.[2]

GENERAL SOLUTION

The dipole of strength c (defined in Part I) is situated at $(0, 0, h)$ with respect to the ground plane $(z=0)$. The Hertz vector at (ρ, ϕ, z) has only a z component and is approximately given by

$$\Pi_z = c\left[\frac{e^{-\gamma_0 r_1}}{r_1} + \frac{e^{-\gamma_0 r_2}}{r_2} - 2\Delta\right] \tag{1a}$$

where

$$\Delta = \int_0^\infty \frac{\gamma_0 \lambda N^{-1} e^{-u_0(z+h)}}{(u_0 + \gamma_0 N^{-1})u_0} J_0(\lambda\rho)d\lambda \tag{1b}$$

for $z>0$ and where

$$r_1 = [(z-h)^2 + \rho^2]^{1/2},$$

$$r_2 = [(z+h)^2 + \rho^2]^{1/2},$$

$$\gamma_0 = i2\pi\lambda_0^{-1},$$

λ_0 = free space wavelength,

$$u_0 = (\lambda^2 + \gamma_0^2)^{1/2}$$

$$N = \eta_0/Z_1 = \gamma_e/\gamma_0,$$

$\eta_0 = 120\pi$, the characteristic impedance of free space, and Z_1 = the normal surface impedance at the surface of the stratified ground.

Eq. (1) in this form is equivalent to (9) of Part I where the integral was evaluated under the restriction that $|z+h| \ll \rho$ and $|\gamma_0\rho| \gg 1$. The first of these can be removed if the integral is evaluated by the method of steepest descents[3] or by the improved saddle point method.[4] The result follows immediately if a new variable of integration α defined by $i\lambda = \gamma_0 \cos\alpha$ is introduced. The integral then has the form

$$\int_C \frac{e^{-\gamma_0(z+h)\sin\alpha} e^{\gamma_0\rho\cos\alpha}(\cos\alpha)^{1/2}}{\cos\frac{\alpha-\alpha_0}{2}\sin\frac{\alpha+\alpha_0}{2}} d\alpha$$

where the leading term of the asymptotic formula for the Bessel function $J_0(\lambda\rho)$ has been employed since it has been assumed that $|\gamma_0\rho| \gg 1$. The contour C is along the negative imaginary axis from $-i\infty$, along the real axis from 0 to π, and then along a line parallel to the positive imaginary axis to $\pi + i\infty$. The pole of the integral is at $\alpha = \alpha_0 + \pi$ where $\alpha_0 = \sin^{-1} 1/N \cong 1/N$. The final result is then given by

$$\Delta = i(\pi p_e)^{1/2} e^{-\bar{p}_e} \operatorname{erfc}(i\bar{p}_e^{1/2}) \frac{e^{-\gamma_0 r_2}}{r_2} \tag{2}$$

where

$$p_e = -\gamma_0 r_2/2N^2 \tag{3a}$$

and

$$\bar{p}_e = -\left[1 - \sin\Phi + \frac{\cos\Phi}{N} + \frac{\sin\Phi}{2N^2}\right]\gamma_0 r_2$$

where

$$\Phi = \tan^{-1}\frac{\rho}{z+h}$$

or

$$\bar{p}_e \cong p_e[1 + N(z+h)/r_2]^2 \text{ for } z+h \ll \rho. \tag{3b}$$

Various aspects of the above result will now be discussed.

THE COMPLEX ATTENUATION FACTOR

If the dipole transmitter and the receiver are on the surface of the ground (i.e. $z=h=0$), the Hertz vector has the following form

---

* Original manuscript received by the PGAP, March 10, 1954; received by the IRE, July 7, 1954. This work was carried out under Project No. D48-95-11-14.

† Radio Phys. Lab., Defence Res. Bd., Ottawa, Can.
‡ Computation Centre, Univ. of Toronto, Toronto, Can.

[1] J. R. Wait, "Radiation from a vertical dipole over a stratified ground, Part I," PGAP TRANS. I.R.E., vol. AP-1, pp. 9–12; 1953.

[2] The notation is the same as that of Part I except where indicated.

[3] P. C. Clemmow, "Some extensions to the method of integration by steepest descents," *Quart. Jour. Mech. and Appl. Math.*, vol. 3, pp. 241–256; 1950.

[4] B. L. Van der Waerden, "On the method of saddle points," *Appl. Sci. Res.*, vol. B-2, pp. 33–45; 1950.

$$\Pi_z = 2ce^{-\gamma_0\rho}\rho^{-1}F_e \tag{4}$$

where F_e is given by

$$F_e = 1 - i(\pi p_e)^{1/2}e^{-p_e}\,\mathrm{erfc}\,(ip_e^{1/2}) \tag{5}$$

and

$$p_e = |p_e|\,e^{ib}.$$

The magnitude of the attenuation factor $|F_e|$ has been tabulated by Norton[5] for $|p_e|$ ranging from 0.001 to 50 and values of b from 0 degrees to -90 degrees. For the case of homogeneous ground as discussed by Norton,[5] the value of b is always less than 0 degrees and the magnitude of F_e never exceeds unity. Since b is defined by

$$e^{ib} = p_e/|p_e| = (Z_1^2/|Z_1^2|)e^{-i\pi/2},$$

it is apparent that b can take positive values for certain types of stratified media. Computations for F_e have therefore been carried out for positive values of b (see Appendix). The function $|F_e|$ is plotted in Fig. 1 for values of $|p_e|$ ranging from 0.001 to 50 and values of b ranging from -90 to $+70$ degrees.

The vertical electric field E_z is given by

$$E_z = -\frac{1}{\rho}\frac{\partial}{\partial\rho}\rho\frac{\partial\Pi_z}{\partial\rho}$$

and since $|\gamma_0\rho| \gg 1$ and F_e is a slowly varying function with respect to ρ it follows that

$$E_z = -2c\gamma_0^2e^{-\gamma_0\rho}\rho^{-1}F_e \text{ for } z = h = 0. \tag{6}$$

For a highly conducting ground where $|p_e| \ll 1$ the electric field is denoted by E_z^∞ and is given by

$$E_z^\infty = -2c\gamma_0^2e^{-\gamma_0\rho}\rho^{-1}. \tag{7}$$

This result can be obtained from elementary methods being just the free space field of an electric dipole of moment $2c$. The factor 2 arises from the imaging of the primary dipole in the perfectly reflecting surface. It is now immediately apparent that under certain conditions where $|F_e| > 1$, the electric field for a stratified ground is greater than the corresponding value E_z^∞ for a perfectly conducting ground.

It is instructive at this point to consider a specific example of ground wave propagation over a two-layer ground with a highly conducting lower layer (i.e. $\sigma_2 \gg \sigma_1$). The transmitter and the receiver are both situated on the surface of the ground at separation ρ so that the numerical distance is given by

$$p_e = -\gamma_0\rho Z_1^2/2\eta_0^2$$

where $z_1 = \eta_1 \tanh \gamma_1 h_1$ and $\eta_0 = 120\pi$. The attenuation factor $|F_e|$ defined by (5) is plotted in Fig. 2 as a function of ρ in kilometers for a relative dielectric constant of the ground equal to 5 (i.e. $\epsilon_1 = 5\epsilon_0$) and a conductivity σ, of 10^{-2} mhos per meter. The operating frequency is

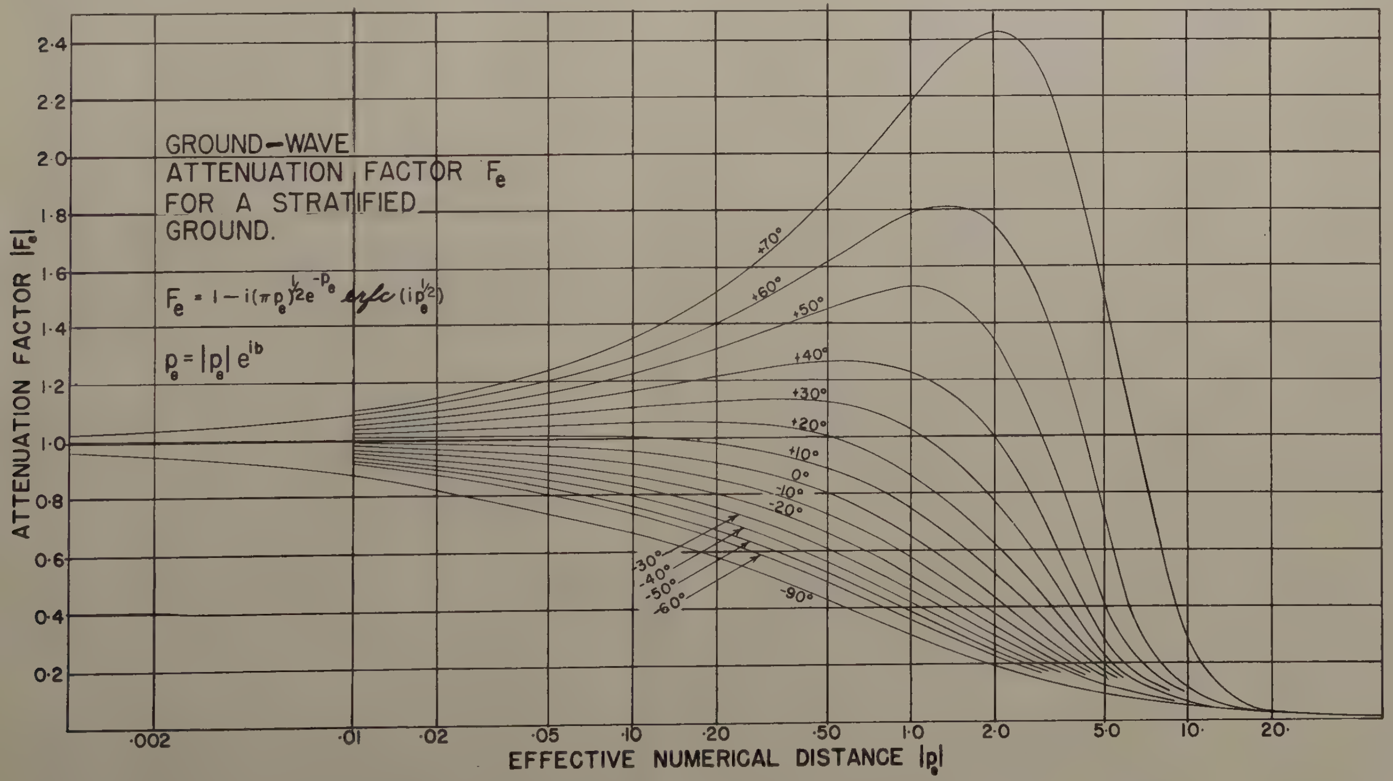

Fig. 1—The ground-wave attenuation factor as a function of the effective numerical distance.

---

[5] K. A. Norton, "The calculation of the ground-wave field intensity," Proc. I.R.E., vol. 29, pp. 623–639; December, 1941.

taken as 10 mc. The thickness of the upper stratum h_1 is shown on the curves. The case where $h_1=\infty$ corresponds to the homogeneous ground. It is very apparent that the attenuation factor exceeds unity for values of h_1 of the order of three feet. On the other hand if h_1 is greater than about six feet the attenuation curves are indistinguishable from those for a homogeneous ground.

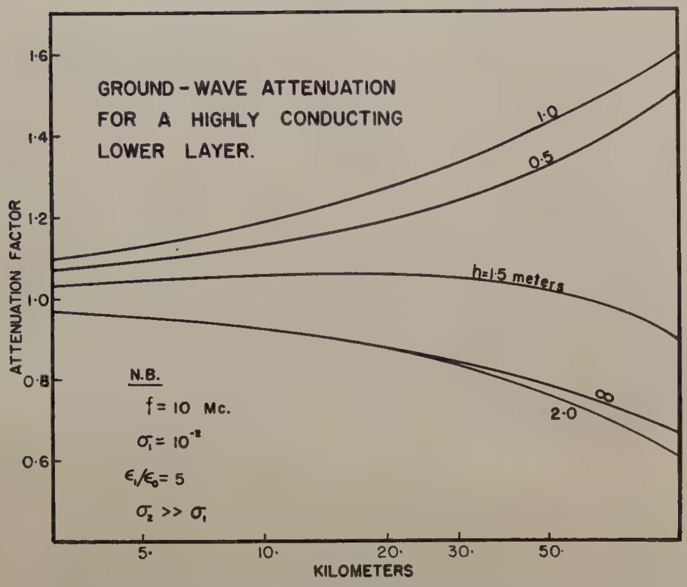

Fig. 2—An example of surface-wave propagation over a two-layer ground where the lower region is highly conducting.

EFFECT OF EARTH CURVATURE

It is well known from the theory of propagation over a homogeneous ground[5] that the earth's surface may be considered a plane if the distance r_1 in kilometers between transmitter and receiver satisfies the inequality

$$r_1 < 50\lambda_0^{1/3}$$

where λ_0 is in meters. This condition is probably equally valid for a stratified ground, since it is determined only by the effective curvature of the earth's surface.

The effect of earth curvature could be evaluated directly by reformulating the problem for a radial electric dipole situated outside a spherically stratified sphere. The solution proceeds in a similar vein to the treatment for the homogeneous sphere.[5] The results for this problem are reserved for a subsequent paper.

APPENDIX

The Complex Attenuation Factor

Values of

$$F_e(p_e) = |F_e|\, e^{i\psi} = 1 - i(\pi p_e)^{1/2} e^{-p_e} \operatorname{erfc}\,(i p_e^{1/2})$$

have been computed on the University of Toronto electronic computer to check the approximate results shown in Fig. 1. The agreement is good.

TABLE I

Amplitude $|F_e|$ Phase ψ

b	$\lvert p_e\rvert=0.03$		b	$\lvert p_e\rvert=3.0$	
0	.987213	−17.56°	0°	.302694	−149.67°
+15°	1.027855	−17.61°	+15°	.388110	−166.34°
+30°	1.070367	−17.34°	+30°	.538230	+176.17°
+45°	1.114022	−16.76°	+45°	.832431	+159.20°
+60°	1.157918	−15.87°	+60°	1.465440	+145.55°
+75°	1.200994	−14.68°	+75°	2.902036	+138.81°
+90°	1.242055	−13.19°			

b	$\lvert p_e\rvert=0.1$		b	$\lvert p_e\rvert=10$	
0	.958061	−31.96°	0°	.060763	−179.76°
+15°	1.031230	−32.33°	+15°	.059438	+160.66°
+30°	1.111889	−32.14°	+30°	.055797	+142.61°
+45°	1.199249	−31.35°	+45°	.050918	+136.55°
+60°	1.291887	−29.94°	+60°	.115585	+142.63°
+75°	1.387625	−27.91°	+75°	.891432	+113.06°
+90°	1.483482	−25.27°			

b	$\lvert p_e\rvert=0.3$		b	$\lvert p_e\rvert=30$	
0	.879799	−54.83°	0°	.0175790	+180.00°
+15°	.997634	−56.31°	+15°	.0175400	+164.16°
+30°	1.139159	−56.82°	+30°	.0174290	+148.40°
+45°	1.306917	−56.27°	+45°	.0172616	+132.79°
+60°	1.502119	−54.53°	+60°	.0170579	+117.38°
+75°	1.723537	−51.54°	+75°	.0168379	+102.16°
+90°	1.966261	−47.27°			

b	$\lvert p_e\rvert=1.0$		b	$\lvert p_e\rvert=100$	
0°	.656482	−96.66°	0°	.0050769	+180.00°
+15°	.811236	−102.29°	+15°	.0050742	+164.77°
+30°	1.030401	−106.55°	+30°	.0050660	+149.56°
+45°	1.343491	−108.95°	+45°	.0050533	+134.38°
+60°	1.790494	−108.96°	+60°	.0050369	+119.24°
+75°	2.420066	−106.08°	+75°	.0050183	+104.16°
+90°	3.280319	−99.91°			

ACKNOWLEDGEMENT

We wish to thank A. P. Dempster, who assisted with the numerical computations.

* * *

A Waveguide Array for Solar Noise Studies*

H. GRUENBERG†

Summary—**A description is given of a 150-foot slotted waveguide array which was built for solar noise studies at wavelengths near 10.3 centimeters. Some of the problems associated with the design of such an array are discussed.**

INTRODUCTION

IN 1950 a project was started at the National Research Council to obtain a high-gain antenna for solar and cosmic noise observations at a wavelength near 10 centimeters. The object was twofold: (1) to get an antenna with sufficient discrimination to be able to scan portions of the sun's surface, and (2) to have sufficient gain to see some of the radio stars which have so far only been observed at much lower frequencies.

It was felt that a half-power beamwidth of one-eighth of a degree, approximately one-quarter of the sun's angular diameter, would be a reasonable compromise between desired discrimination and required antenna size. A parabolic reflector which would produce a pencil beam as narrow as that in both the *E*-plane and the *H*-plane has to have a diameter of about 170 feet. The cost of such a project would be rather large, especially when the reflector has to meet resasonably close tolerances and when some sort of suspension has to be provided to direct the antenna beam to any desired portion of the sky. It was decided, therefore, to build a linear slotted-waveguide array 150 feet long, fitted with a suitable horn to obtain a beaver-tail beam. The array was to be positioned in an East-West direction and made rotatable about a longitudinal axis so that the beam could be directed at points close to the meridian, but of arbitrary elevation.

By the use of such an array the angle discrimination in the azimuthal direction can still be made the same as in the case of the parabolic reflector, but the beamwidth in the vertical direction would be much larger and the antenna gain would be reduced considerably. Nevertheless, an effective gain of the order of 10,000 could be expected. So far no radio stars have been observed at wavelengths of about 10 centimeters, but the present array has turned out to be a very useful tool for studying solar radiation.

DESIGN CONSIDERATIONS

A design wavelength of 10.3 centimeters was selected. This makes a 150-foot array approximately 450 wavelengths long. In terms of wavelengths it is believed to be the longest waveguide array built so far. Such a long array requires careful design both electrically and mechanically. This was especially true since it was planned to design the array in such a way as to make doubling or even tripling of the length possible at a later date.

To meet the last requirement, it was necessary to have all slots in the array equally excited. Such a uniform excitation along the array leads to a maximum sidelobe level of 4 per cent in terms of power relative to the main beam. This is not too serious in the present application. To avoid mutual coupling between slots and to simplify the design procedure, longitudinal shunt slots in the broad face of a rectangular waveguide were used as the radiating elements. The phase and amplitude of excitation for such slots can be easily and independently adjusted by proper spacing along the array and by proper slot offsets from the center line of the guide face. In calculating the slot offsets for such a long array, attenuation in the waveguide must be taken into consideration.

To get satisfactory operation over a reasonable frequency band, the array cannot be of the resonant-spaced type. A slot spacing near 220 electrical degrees was chosen. With the usual staggering of the slots about the center line of the guide this gives rise to about 40 degrees phase shift between slots and a squint angle of about 7 degrees between the main beam and array normal or meridian plane. This squint angle will change with frequency and this will cause an effective broadening of the beam depending on the bandwidth of the IF amplifier used in the receiver.

A number of other factors will affect the performance of the array. Dimensional tolerances of the waveguide selected and machining tolerances will modify the radiation pattern to be expected. Ambient temperature fluctuations may not seriously affect the electrical performance, but the accompanying differential thermal expansions and contractions must be taken into account in the mechanical design and hence, also, to some extent, in the electrical design.

ELECTRICAL DESIGN

Consider an array of N shunt slots, the distance between consecutive slots being constant and equal to d. Let the slots be numbered from 1 to N. If the slots are of resonant length, their effect in the waveguide may be represented by pure shunt conductances across an equivalent transmission line. In a long array (i.e. for large values of N) these conductances are small compared to the characteristic admittance of the line and we may assume that the line is approximately matched at each slot,[1] if the line has a matched termination. The power extracted from the traveling wave in the guide by each slot is then proportional to the normalized slot conductance and to the power incident on the slot.

Let f_n be the desired amplitude of excitation of the n^{th} slot and let the units be chosen so that f_n^2 represents

---

* Original manuscript received by the PGAP, October 19, 1953; received by the IRE, July 7, 1954.

† Associate Research Officer, Radio and Elec. Eng. Div., National Research Council, Ottawa, Can.

[1] W. H. Watson, "Physical Principles of Wave Guide Transmission and Antenna Systems," Clarendon Press, Oxford, Eng., p. 130; 1947.

the power radiated by the n^{th} slot for unit power input into the first slot. Then, in the case of a lossless line, the normalized slot conductances g_n are given by

$$f_1^2 = g_1, \qquad f_n^2 = g_n\left(1 - \sum_1^{n-1} f_k^2\right). \tag{1}$$

The power that reaches the termination is

$$P_L = 1 - \sum_1^N f_k^2$$

and is usually made equal to from 5 to 10 per cent of the input power to insure the approximately matched condition all along the line. The f's must therefore be normalized to obtain the selected array efficiency

$$\eta = \sum_1^N f_k^2 = 1 - P_L. \tag{2}$$

Substituting (2) in (1), one obtains

$$g_n = \frac{f_n^2}{(1/\eta)\sum_1^N f_k^2 - \sum_1^{n-1} f_k^2}, \qquad n > 1. \tag{3}$$

The conductance of the last slot becomes

$$g_N = \frac{f_N^2}{P_L + f_N^2}. \tag{4}$$

For long arrays, especially for those with the usual tapered amplitude distributions, the last expression becomes approximately

$$g_N = f_N^2/P_L. \tag{5}$$

In (1) to (5) it is assumed that losses in the waveguide can be neglected. In the present application this is not possible. If d is the slot spacing and α the attenuation in the guide in decibels per unit length, then the fractional decrease of energy between successive radiators is

$$\delta = e^{-0.230\alpha d} \cong 1 - 0.230\alpha d. \tag{6}$$

When this loss is taken into consideration, it is easily shown that the above equations become

$$f_1^2 = g_1, \quad f_n^2 = g_n\delta^{n-1}\left(1 - \sum_1^{n-1} f_k^2\delta^{1-k}\right) \tag{1a}$$

$$P_L = \delta^{N-1}\left(1 - \sum_1^N f_k^2\delta^{1-k}\right) \tag{2a}$$

$$g_n = f_n^2\delta^{1-n}\left(\frac{\delta^{N-1}}{\delta^{N-1} - P_L}\sum_1^N f_k^2\delta^{1-k} - \sum_1^{n-1} f_k^2\delta^{1-k}\right)^{-1}, \qquad n > 1. \tag{3a}$$

Eqs. (4) and (5) remain unaltered.

For uniform excitation, $f_1 = f_2 = \cdots = f_N = f$, the normalized conductance of the n^{th} slot becomes

$$g_n = \frac{\eta}{N - (n-1)\eta} \tag{7}$$

for a lossless guide, and

$$g_n = \frac{1-\delta}{\delta^n}\left(1 - \delta^{1-n} - \frac{1 - \delta^{-N}}{1 - P_L\delta^{1-N}}\right)^{-1} \tag{7a}$$

when the guide losses are included.

Power Gain and Optimum Length

As stated above, it is planned to increase the length of the array at a later date. It is clear, however, that there is not much sense in increasing the length indefinitely apart from the fact that construction tolerances become more severe at longer lengths. Although antenna directivity increases with length, the power gain (directivity × array efficiency) eventually starts to drop off because of increased waveguide losses.

The efficiency of a long uniformly-excited array with guide losses is, from (2), (5), and (7a):

$$\begin{aligned}\eta &= \sum_1^N f_k^2 = Nf_N^2 = P_L N g_N \\ &= \frac{P_L N(1-\delta)(1 - P_L\delta^{1-N})}{(1-\delta) + P_L\delta(1 - \delta^{1-N})}.\end{aligned} \tag{8}$$

The power gain can be obtained from the efficiency by multiplying by the directivity which is proportional to the length of the array and hence to N. It will be of the form

$$G \propto \frac{N^2(\delta^N - A)}{\delta^N - B} \tag{9}$$

where

$$A = P_L\delta \cong P_L, \qquad B = \frac{P_L\delta^2}{1 - \delta + P_L\delta} \cong \delta \cong 1. \tag{10}$$

By differentiation with respect to N, the condition for maximum gain becomes

$$e^{-x} + P_L e^x + x(1 - P_L)/2 = 1 + P_L \tag{11}$$

where x is related to the array length L by

$$x = 0.230\alpha dN \cong 0.230\alpha L.$$

Here, use was made of the approximations in (10). These simplifications are justified in all practical cases. For 5 and 10 per cent of the input power going to the termination, (11) is satisfied by $x = 1.24$ and $x = 1.03$, respectively. This leads to optimum array lengths for brass S-band waveguide ($\alpha = 0.012$ db/feet) of 450 and 375 feet. For silver or copper guides the corresponding optimum lengths would be about twice as large. It is easily seen from the above that when the length of an array is increased beyond the optimum values given, the gain drops until it vanishes for $1 - P_L\delta^{1-N} = 0$, or $L = (1/0.230\alpha)\ln(1/P_L)$. All the input power is now dissipated in the waveguide and the termination, and all slots have zero conductance and do not radiate. This is forced to be the case since each slot is given equal power which by above conditions slot power→0 as $L \to \infty$.

It can be seen that the 150-foot brass waveguide array is well below optimum length. It has an over-all efficiency, including the 10 per cent loss in the termination, of about 68 per cent. Extension of the array to 300 feet would double the resolution, but lower the efficiency to 58 per cent. Hence the power gain would only be increased by 70 per cent. The power left over in the termination would be reduced to 4.2 per cent. A further improvement in gain (a little more than 10 per cent) would be possible by using a silver-plated guide. This improvement was considered too small in view of the extra cost.

BEAM WIDENING DUE TO INTERMEDIATE-FREQUENCY BANDWIDTH

A linear array of N isotropic radiators, with constant spacing d and constant phase shift ψ between consecutive radiators, has a field strength radiation pattern[2]

$$E_0(\theta) = \frac{\sin \left| \tfrac{1}{2}N(\beta d \sin \theta - \psi) \right|}{N \sin \left| \tfrac{1}{2}(\beta d \sin \theta - \psi) \right|} \tag{12}$$

where $\beta = 2\pi/\lambda$ and the angle θ is measured from the array normal. In the type of array considered, $\psi = 2\pi d/\lambda_g - \pi$. ($\lambda$ and λ_g are the free-space and guide wavelengths, respectively.) The pattern has a maximum at an angle θ_0 given by[3]

$$\begin{aligned} \sin \theta_0 &= \lambda/\lambda_g - \lambda/2d \\ &= [1 - (\lambda/2a)^2]^{1/2} - \lambda/2d \end{aligned} \tag{13}$$

where a is the width of the guide. For long arrays, the field strength has significant values only for small values of θ, the assumption of isotropic radiators becomes unimportant and one may write, approximately,

$$E_0(\theta) = \frac{\sin \left| (\pi L/\lambda)(\theta - \theta_0) \right|}{(\pi L/\lambda)(\theta - \theta_0)} \cdot \tag{14}$$

This leads to a half-power beamwidth of $50.8\lambda/L$ degrees. The 150-foot array will have a theoretical beamwidth of 0.116 degrees at the design wavelength.

So far the effect of IF bandwidth has been neglected. Since the squint angle θ_0 is a function of frequency, the peak powers received at the different frequencies in the IF band will come from slightly different directions at a given time. As the squint angle variation with frequency is almost linear, each frequency component within the IF band will have associated with it a pattern almost identical with the above except for a displacement in angle which can be computed from (13) and is given by

$$\xi = k(\Delta f/f_0), \qquad k = (\lambda_g/\lambda)_0 - \theta_0. \tag{15}$$

Here Δf is a deviation from the design frequency f_0, and k is a constant evaluated at the design frequency. For the array described in this paper, $k = 1.30$ radians $= 75$ degrees. Assuming a rectangular bandpass, w cycles wide, and constant signal amplitude within that band, the composite radiation pattern will have the form

$$E^2(\theta) \propto \int_{-kw/2f_0}^{kw/2f_0} \frac{\sin^2 \left[(\pi L/\lambda)(\theta - \theta_0 - \xi)\right]}{\left[(\pi L/\lambda)(\theta - \theta_0 - \xi)\right]^2}\, d\xi. \tag{16}$$

The square of the amplitude is integrated over the frequency range because the square-law detector averages to zero all cross products of different frequency components. The integral in (16) can be evaluated by the substituting $x = (\pi L/\lambda)(\theta - \theta_0 - \xi)$ and integration by parts. The result, normalized to unity at the peak, which still occurs at $\theta = \theta_0$, is

$$E^2(\theta) = \frac{Si\,[2(x_0 + u)] - Si\,[2(x_0 - u)] + \dfrac{[u(1 - \cos 2x_0 \cos 2u) - x_0 \sin 2x_0 \sin 2u]}{(x_0^2 - u^2)}}{2\,Si\,2u - (1 - \cos 2u)/u} \tag{17}$$

where

$$x_0 = (\pi L/\lambda)(\theta - \theta_0), \qquad u = (\pi L/\lambda)(kw/2f_0). \tag{18}$$

As $w \to 0$, this expression reduces to (14). As the IF bandwidth increases, (17) shows that the radiation pattern broadens and also that the nulls in the pattern are filled in.

In actual practice, the IF bandpass is, of course, not rectangular. To assess the effect of the shape of the response curve of the IF amplifier, the integrand in (16) must contain an appropriate weighting factor. The integration was carried out numerically for the actual measured power response curve of the IF amplifier. The expected beamwidths are shown in Fig. 1, page 150, as a function of IF bandwidth. Fig. 1 also shows the beamwidth deduced from the analysis of solar observations.

It is not feasible to measure the radiation pattern of the 150-foot array directly, but experimental patterns have been deduced from observations of sun spots.[4] These agree quite well with the expected pattern (Fig. 2, page 150).

FACTORS AFFECTING THE BEAM POSITION

In theory, the peak of the main beam points in a direction which deviates from the array normal by the squint angle given in (13). Experimentally, a small discrepancy was observed from the theoretical results. In the derivation of (13) it is assumed that the slots act as

---

[2] W. R. Smythe, "Static and Dynamic Electricity," McGraw-Hill Book Company, Inc., New York, N. Y., p. 484; 1950.

[3] Watson, *op. cit.*, p. 129.

[4] A. E. Covington and N. W. Broton, "Brightness of the solar disc at a wavelength of 10.3 centimeters," paper presented to the Spring Meeting of URSI, held in Washington, D. C., April, 1954. *Astrophys. Jour.*, vol. 119, pp. 569–589; May, 1954.

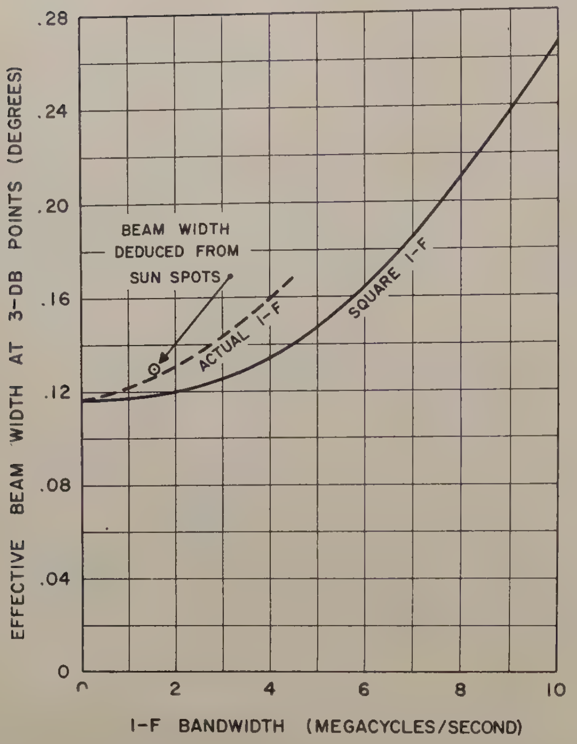

Fig. 1—Dependence of effective beamwidth on the IF bandwidth.

pure shunt conductances across an equivalent transmission line and that the magnitude of these conductances is small compared to the characteristic admittance of the line. These assumptions are usually quite good in the case of a long array, but they still only approximate the true situation. There is some doubt as to the true resonant length of the slots, and the loading of the line by the slot conductances is small but not negligible. Furthermore, although longitudinal slots in the broad face of the guide closely act as pure shunt elements, their exact representation requires small series reactances in an equivalent *T*-network. These series elements will produce additional small phase shifts from slot-to-slot, which may also affect the beam position slightly.

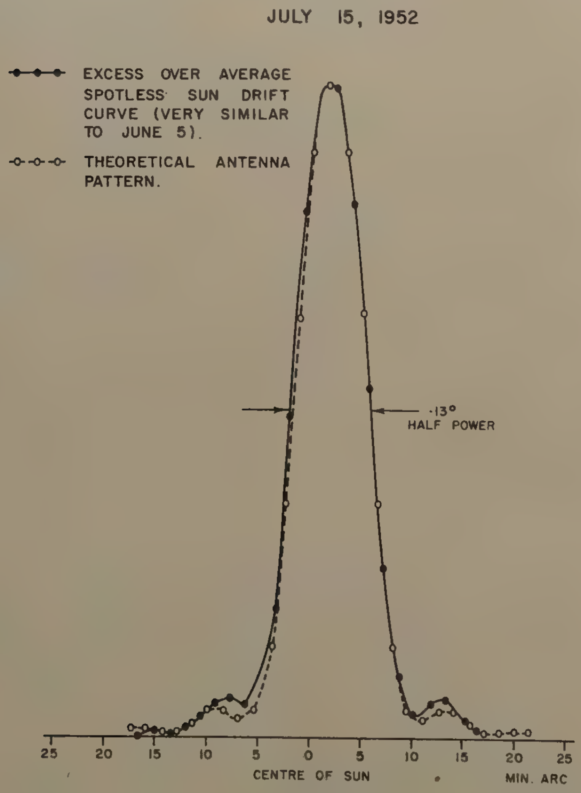

Fig. 2—Theoretical and experimental radiation patterns.

The squint angle can be measured very accurately to ±1 minute of an arc, by timing the transit of the sun, since great care was taken to locate the array axis in a level East-West direction. The usual corrections for local time and equation of time must be applied. Since squint and hour angle are equal only when the sun is on the equator, the declination of the sun must be taken into consideration. Refraction of electromagnetic waves in the atmosphere produces a small correction, much less than one minute of an arc.

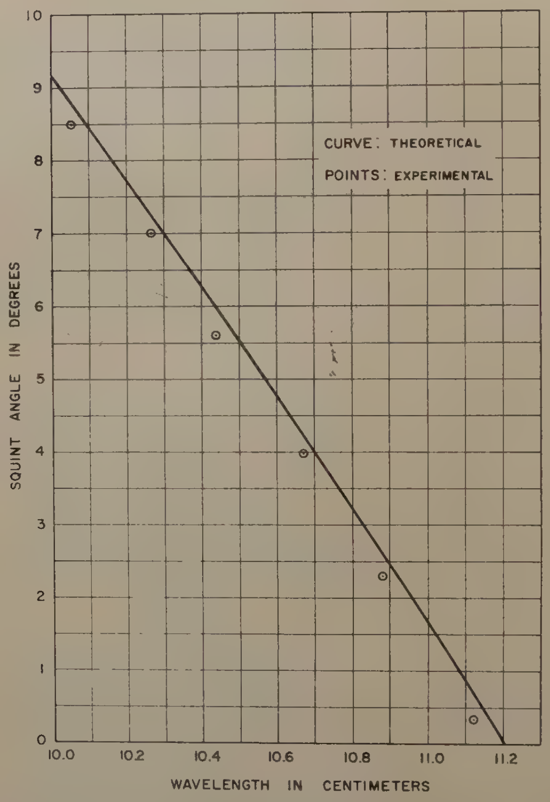

Fig. 3—Variation of squint angle with frequency.

Fig. 3 shows the theoretical variation of squint angle with operating wavelength and some experimental points. There appears to be a nearly constant discrepancy of about a quarter of a degree. The experimental results show very little variation during the course of a year (not more than ±2 minutes of an arc). This shows that the discrepancy is independent of the zenith distance of the sun which provides a check on the accuracy of the level East-West alignment of the array.

A number of possible causes for the above discrepancy were investigated. Since the squint angle is a function of the guide-width and the slot-spacing, the effect of mechanical tolerances and temperature variations must be considered. It is easily shown from (8) that average variations Δa and Δd in guide-width and slot-spacing, and temperature changes Δt produce the following beam shifts:

$$\Delta\theta_0 = \frac{(\lambda/2a)^2}{[1-(\lambda/2a)^2]^{1/2}} \frac{\Delta a}{a} \tag{19}$$

$$\Delta\theta_0 = \frac{\lambda}{2d} \frac{\Delta d}{d} \tag{20}$$

$$\Delta\theta_0 = \left\{\frac{\lambda}{2d} + \frac{(\lambda/2a)^2}{[1-(\lambda/2a)^2]^{1/2}}\right\} \alpha_t \Delta t. \tag{21}$$

Here α_t is the coefficient of thermal expansion of the waveguide material. An average error of ±0.002-inch in the guide-width will change the squint angle by about ±1.7-minutes of an arc. A similar error in the average slot-spacing or an error of $\pm\frac{1}{2}$-inch in the over-all array length can only account for about ±1 minute. Extreme temperature variations during the year will account for not more than 2 or 3 minutes. In any case, temperature corrections were applied to all experimental data.

Another possible source of error is in the measurement of frequency. However, the frequency is believed to be known to ±0.3 mc per second, while an error of about 10 mc would be required to explain the discrepancy in squint angle. The local oscillator frequency was measured by two precision cavity meters and also by a wavemeter of the coaxial type. The intermediate frequency (about 30 mc per second) was also carefully measured. It was also checked indirectly by observing transits of the sun at both image frequencies. The difference in squint (about 1.5 degrees) is, of course, related to twice the intermediate frequency by the slope of the squint-wavelength curve.

The above discussion seems to indicate that the small discrepancy between measured and calculated squint angles must be due to one or more of the assumptions inherent in (13) as mentioned at the beginning of this section. Errors in the resonant length of the slots and loading of the line by the shunt conductances do not provide good explanations. The first would cause a phase shift between radiated field and the field exciting the slots.[5] This phase shift would, however, be about the same for all slots and hence would not shift the beam. Shunt loading of the line should have no effect for resonant spacing of the slots, but experiments indicate a constant discrepancy right up to resonant spacing. The most likely cause is the neglected series impedances in the T-representation of the slots. These could easily produce the additional phase shift (about 1.4 electrical degrees) between consecutive slots required to explain the above mentioned discrepancy. It is also feasible that this phase shift is reasonably independent of the wavelength over the range considered since resonances in the series elements of the T will not occur at the same frequency as those in the shunt element. Unfortunately, it is rather difficult to measure such a small phase shift directly so that this explanation is somewhat open to question.

MECHANICAL CONSTRUCTION

The array was constructed from fifteen 10-foot sections of standard S-band brass waveguide ($1\frac{1}{2}$ inches by 3 inches outside dimensions, 0.080-inch wall thickness). These sections were carefully selected for uniformity in internal dimensions. The spacing, d, between slots was chosen as 3.500 inches to give a beam squint, θ_0, of about 7 degrees at the design wavelength of 10.3 cm. The decrement, δ, and the slot conductances, g_n, were then calculated from (6) and (7a). A terminal loss of 10 per cent was assumed. Slot offsets were computed from Stevenson's formula[6] and dimensions were chosen from experimental curves to make the slots resonant at the design wavelength. A horn of 60 degrees total flare-angle, having an aperture width of 18 inches, was fitted along the entire length of the guide to reduce the beamwidth in the transverse plane and to increase the antenna gain. Measurements on a short mock-up gave a half-power beamwidth of about 20 degrees in the transverse plane.

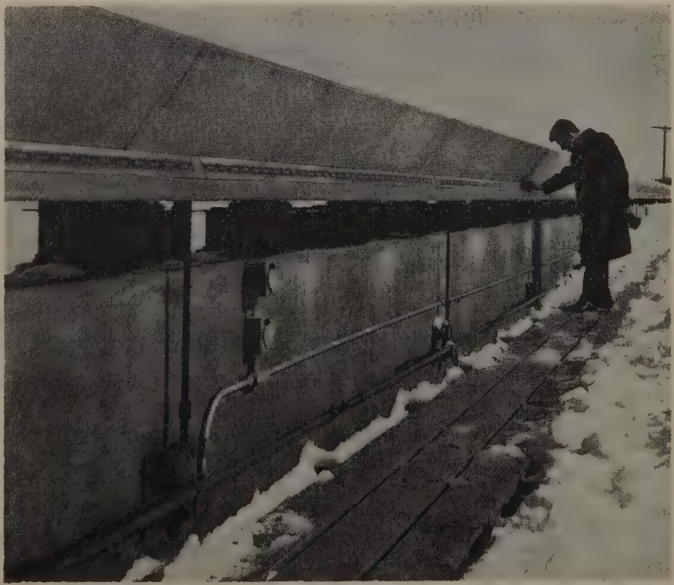

Fig. 4—Photograph of a section of the array.

The array is mounted in a level East-West position on a long steel shaft which allows the entire antenna to be rotated along a longitudinal axis (see Fig. 4). The shaft is held in carefully aligned bearings mounted on a reinforced concrete pier, and the pier is in turn anchored on bedrock.

---

[5] R. J. Stegen, "Slot radiators and arrays at X-band," PGAP TRANS. I.R.E., pp. 62–84; February, 1952.

[6] A. F. Stevenson, "Theory of slots in rectangular wave guides," *Jour. Appl. Phys.*, vol. 19, pp. 24–38; 1948.

CONCLUSION

Since an analysis of the data on solar observations will be presented elsewhere,[4] this phase has been entirely omitted from this paper. It will suffice to mention that these observations indicate that the array is working satisfactorily over a wavelength range from about 10.0 to 11.0 cm. The input voltage standing-wave ratio was below 1.1 for wavelengths between 10.1 and 10.9 cm. The beamwidth and beam shape deduced from sun spot observations agrees well with the design objectives. The variation of squint angle with wavelength is as predicted except for a small constant discrepancy, about 15 minutes of an arc, which can most likely be explained by the fact that the small series elements in the equivalent-*T* representation of the slots have been neglected.

The power gain at the design wavelength, as estimated from the half-power beamwidths in the *E*-plane and *H*-plane (22.5 and 0.13 degrees, respectively) and from the theoretical efficiency, is about 10,000. Direct measurement of the gain by comparison with a 4-foot parabolic reflector and the use of a standard noise source[4] gave a power gain of 7,300. Since the measured amplitude distribution along the array and the power left in the termination agreed reasonably well with the design objectives, it is fair to assume that this discrepancy is due to a small increase in the general level of spurious radiation in directions other than that of the main beam. Inaccuracies in mechanical construction can easily produce an average increase of half a per cent in the sidelobe level which is sufficient to account for the discrepancy.

ACKNOWLEDGEMENT

The author wishes to express his thanks to his associates in the Radio and Electrical Engineering Division, in particular to Dr. G. A. Miller, A. E. Covington and N. W. Broten; and to H. E. Parsons and Z. Mordasewicz, who carried out the mechanical design and supervised the construction.

Dielectric Sheet Radiators*

F. E. BUTTERFIELD†

***Summary*—A class of electromagnetic radiators is described which employs the principle of waveguiding along a flat surface by means of dielectric coating. Radiation occurs as a result of nonuniformities in the guiding system. The efficiency of the feeding arrangements and diffraction over the edge of the flat surface are factors in the side-lobe level observed. A unit is described which has been used aboard missiles.**

A series of tests are reported which illustrate some of the characteristics of the radiators. Data for comparison with corrugated surface antennas is given. Problems for further investigation are listed.

An experimental unit is described with a gain of 25 db and an efficiency compared to conventional aperture radiators of about 60 per cent. This unit has linear dimensions comparable to a horn producing the same beamwidth.

INTRODUCTION

FOR RADIATION nearly normal to a surface, such as the skin of an aircraft or missile, arrays of slots with transparent covers have sufficed. For nearly tangential radiation, however, slot arrays become difficult to build.

Practical tangentially-directed antennas have been constructed for use aboard missiles by using dielectric coatings on the surfaces involved. Some description of their operation and performance will aid in their evaluation. Furthermore, it will help to relate the various viewpoints which are being taken concerning these and similar units.

WAVEGUIDING IN DIELECTRIC SHEETS

Waveguiding by dielectric slabs or sheets is easily demonstrated by connecting two metal waveguides by a metal surface and a dielectric sheet as shown in Fig. 1. The efficiency of transmission is found to be greatly dependent upon conditions at the ends of the dielectric and much less dependent upon those at the center. If the sheet is uniformly thick and of uniform width, the power transmitted is proportional to thickness for a considerable range of thickness. If metal sides are raised on the sides of the dielectric, however, cutoff will be experienced for narrow, thick dielectrics.

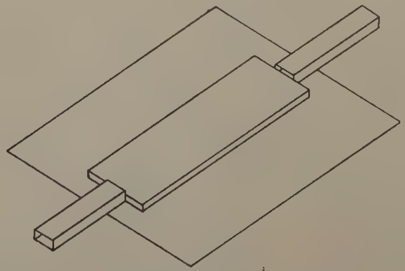

Fig. 1—Dielectric sheet waveguide.

---

* Original manuscript received by the PGAP, February 9, 1954; revised manuscript received, June 24, 1954; received by the IRE, July 7, 1954.

† Motorola, Inc., Phoenix, Ariz.

The capabilities of plane dielectric-coated surfaces to guide waves have been analyzed by Attwood.[1] A more complete description of surface waves has been given by Barlow and Cullen.[2]

Attwood expressed the simple case of the unrestricted sheet in terms of a number of wave constants k_2, k_3, β, K_z, v/c, and the contour which encloses 90 per cent of the transmitted power. The y directed propagation constants for the wave inside and outside the dielectric are k_2 and k_3, respectively. The phase constant in the direction of propagation is β. The current in the metal surface per unit width is K_z. The ratio between wave velocity and the velocity of light is v/c.

Use can be made of these quantities to establish a new quantity, A, which is the proportion of total power that flows in the dielectric. These quantities are complicated functions of the thickness, a, of the dielectric. They are plotted in Fig. 2 along with E_{za}, the tangential field in the propagating direction at the dielectric surface for the particular case of $f=10$ kmc, $\epsilon_{r2}=4$.

Restriction of the sheet to a finite width normal to the direction of propagation, results in the wave being hybrid. Furthermore, the wave spreads laterally and occupies space on both sides as well as above the dielectric. The wave velocity on these strips of dielectric is different from that shown in Fig. 2 by a small amount but never reaches the free space velocity. It is this "slow wave" characteristic that prevents radiation just as in the related ~~systems~~ of dielectric wires[3] and metal helixes.

Although Attwood's solution does not cover the case of the narrow dielectric strip, it gives sufficient information to describe the dielectric sheet antenna operation.

In Fig. 2, for thickness, a, greater than 7 mm, nearly all the power flows inside the dielectric. The thickness for which 90 per cent to 98 per cent of the power is inside the dielectric appears to be capable of suitably loading a metal waveguide for feeding purposes.

This is not an inconvenient dimension for mechanical connection to a rectangular guide. The match under these conditions can be adjusted to any desired degree by the use of a short taper or a step transition in a section of dielectric projecting into the guide. This dielectric plug provides an opportunity to seal the waveguide if this is required.

The efficiency with which the wave is converted from the *TE* mode of the hollow metal guide to the hybrid mode of the surface wave may be less than 100 per cent. In this case some radiation is produced at the junction. Proper control of dimensions near the junction reduces this radiation so that it becomes less important in dielectric sheet antennas than the radiation resulting from nonuniformity of the dielectric.

DIELECTRIC SHEET ANTENNAS

Recent work in surface wave radiators has been concerned principally with corrugated surfaces for wave guiding.[4]

Circular antennas that depend upon this type of wave transmission on coated surfaces have been used since 1950 at least.[5,6] End fire antennas have been described by Ehrlich and Newkirk,[4] and by Ohio State University Research Foundation,[7] but in general only.

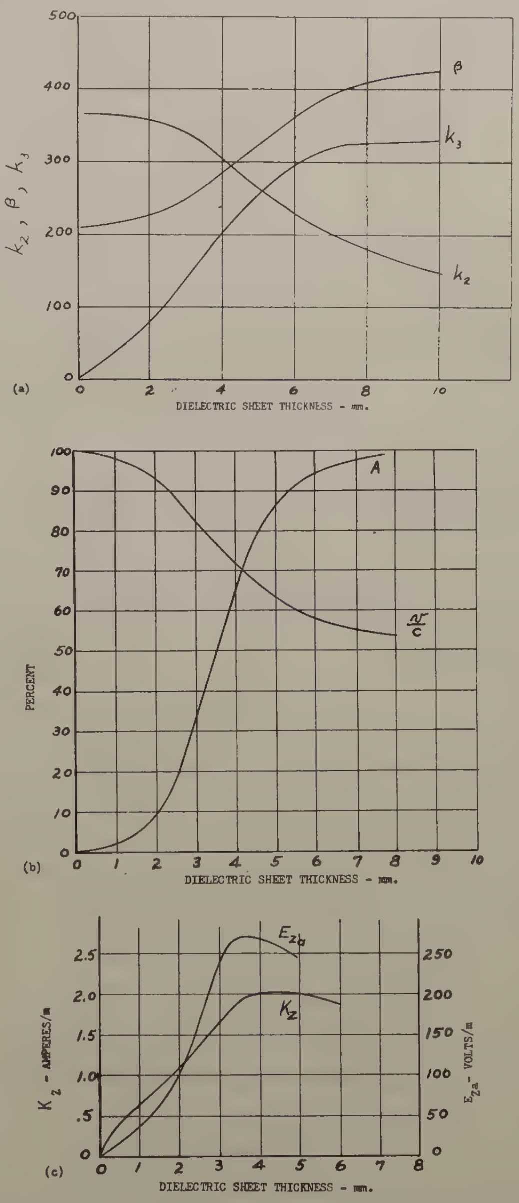

Fig. 2—Constants for propagation of surface-guided wave by dielectric sheet on metal surface. 10 kmc. $\epsilon_r=4$.

---

[1] S. S. Attwood, "Surface-wave propagation over a coated plane conductor," *Jour. Appl. Phys.*, vol. 22, pp. 504–509; April, 1951.

[2] H. M. Barlow and A. L. Cullen, "Surface waves," *Proc. IEE*, part III, vol. 100, pp. 329–341; November, 1953

[3] D. D. King, "Dielectric image line," *Jour. Appl. Phys.*, vol. 23, pp. 699–700; June, 1952.

[4] M. J. Ehrlich and L. L. Newkirk, "Corrugated Surface Antennas," 1953 CONVENTION RECORD OF THE I.R.E., part 2, pp. 18–33.

[5] D. W. Fry and F. V. Goward, "Aerials for Centimetre Wavelengths," Cambridge University Press, New York, N. Y., p. 156; 1950.

[6] E. M. T. Jones and R. A. Falsom, Jr., "A note on the circular dielectric-disc antenna," PROC. I.R.E., vol. 41, p. 798; June, 1953.

[7] Ohio State Univ. Res. Foundtn., Columbus, Ohio. Eng. Rep. No. 486-1, February 15, 1952; Contract No. AF 18(600)85 E.O. Nos. 112-110 SR6f2 112-105SJ-913, "Flush Mounted Antennas for Direction Finding and ECM."

Fig. 3 shows suppressed and unsuppressed forms of a dielectric sheet radiator. These two forms are very nearly equal in performance. This figure also shows the co-ordinate system to be used in the description of the characteristics of this antenna.

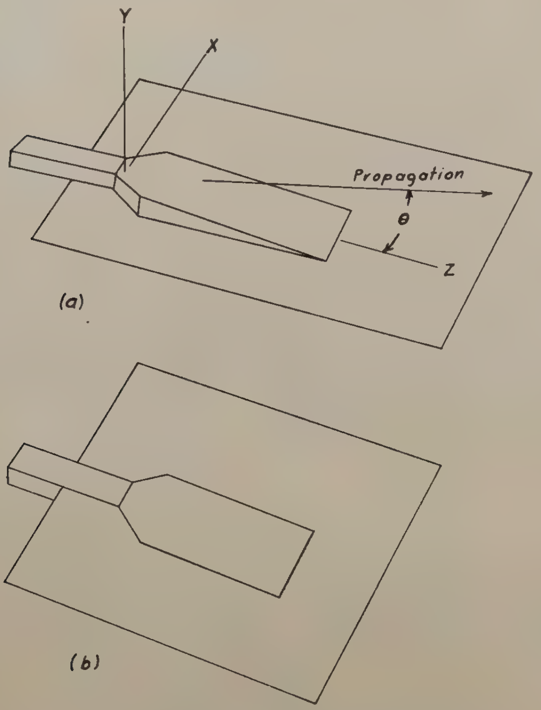

Fig. 3—Two methods of applying dielectric sheets to surfaces to form antennas.

The purpose of an antenna is to provide a distribution of field over a large aperture as efficiently as possible. Wide distribution of field in dielectric sheet transmission systems is associated with thin dielectric layers. Good termination to feeding waveguides is associated with thick layers. The design of a dielectric sheet antenna is largely the design of a tapering transmission system between these two end requirements. From Attwood's paper, the power outside the dielectric is

$$P_{z3}\Big|_{y=d}^{\infty} = -\frac{1}{2}\int_{y=d}^{\infty} (E_{y_3}H_{x_3}^{*})_{\text{real}}\,dy$$

where d is any distance above the metal surface.

$$= \frac{1}{2}\int_{y=d}^{\infty} K_z^2 \frac{k_2^2}{k_3^2}\,\frac{\beta}{\omega\epsilon_2^2}\,\epsilon_3 e^{2k_3a}\sin^2(k_2a)e^{-2k_3y}dy$$

$$= M\int_{y=d}^{\infty} e^{-2k_3y}dy = \frac{M}{2k_3e^{2k_3d}}$$

where

$$M = K_z^2\frac{k_2^2}{k_3^2}\,\frac{\beta}{\omega\epsilon_2^2}\,\epsilon_3e^{2k_3a}\sin^2(k_2a).$$

Define A so that

$$P_{z3}\Big|_{y=a}^{\infty} = (1-A)P_t$$

where P_t is the total power.

Define $m<1$, so that

$$mP_{z3} = \Big|_{y=a}^{\infty} = P_{z3}\Big|_{y=d}^{\infty};$$

then

$$\frac{Mm}{2k_3e^{2k_3a}} = \frac{M}{2k_3e^{2k_3d}}$$

$$d = a + \frac{\log\frac{1}{m}}{2k_3}.$$

This expression gives the power contours outside the dielectric in terms of the dielectric thickness and the parameter, m. Let $m=C/100(1-A)$, where C is the power percentage of interest ($C=10$, 20, ——100 per cent). Corresponding values of d are on the 10 per cent, 20 per cent,——100 per cent contours of total power.

Fig. 4 shows power contours for a uniform taper in infinitely wide sheet. The rate of field expansion near the thin end is extreme. Fig. 5 shows power contours for a nearly exponential taper to an end thickness of 0.5 mm. The rate of field expansion is more uniform. The exponential nature of the optimum taper has been verified experimentally. Two rather clearly defined areas are involved: one primarily releases energy, the other primarily guides it.

An important consideration in end fire array design is the total phase shift between fields radiated by elements at the ends of the array. For maximum gain with uniformly excited elements, this shift should be $2\pi l/\lambda + \pi$ radians.[8] This requirement holds for dielectric sheet radiators also. The unit is made long enough for this condition to be approximated.

Side-lobe level is as important a consideration in antenna performance as gain in certain applications. The maximum gain uniform end fire array has side lobes down 10 db from the main lobe. These side lobes may be reduced if necessary by tapering the array element excitations (all other array constants remaining fixed), and side-lobe level is improved at the expense of gain. The first side lobes may be reduced in dielectric sheet radiators by adjustments in the dielectric thickness in the energy releasing area of the sheet. This effectively shortens the radiator, broadens the pattern, enhances the small, wide angle side lobes, and reduces the gain of the antenna.

A recent development has appeared[9] by which illumination taper and phase delay along the array can be more intimately related in order to obtain greater gain. Investigation of the application of this material to dielectric sheet antennas has not yet been made.

[8] W. W. Hansen and J. R. Woodward, "A new principle in directional antenna design," Proc. I.R.E., vol. 26, pp. 333–346; March, 1938.

[9] A. Block, R. G. Medhurst, and S. D. Pool, "A new approach to the design of super directive aerial arrays," *Proc. IEE*, part III, vol. 100, pp. 303–314; September, 1953.

In the consideration of side lobes, two other factors are involved: (1) radiation from the end of the feeding waveguide, and (2) diffraction. If the feeding waveguide radiates independently of the dielectric sheet, interference maximum and minimum, or side lobes, occur. This usually undesirable feedguide radiation can be minimized by proper dielectric dimensions and other details near the feed end.

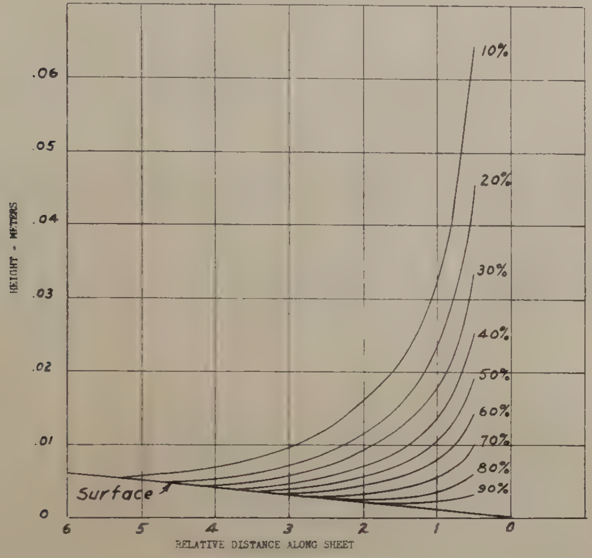

Fig. 4—Power contours for wave guided dielectric sheet of uniform taper.

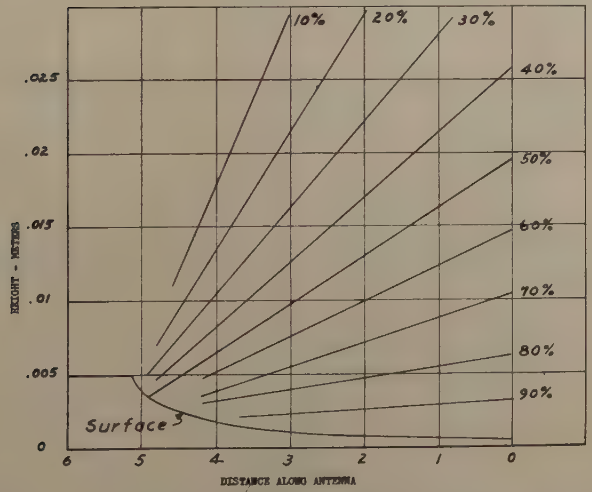

Fig. 5—Power contours for wave guided by dielectric sheet with approximately exponential taper.

The role of diffraction is well known.[10] It must be emphasized for applications where the metal surface involved has a boundary cutting across the direction of propagation. All vehicles fall into this category. Diffraction maxima and minima must be expected even in directions at large angles to the sheet. The maximum radiation makes a small angle with the tangent to the surface and the intensity drops off smoothly on the side of the surface opposite the radiator. The surface edge need not be a sharp ending to produce this effect; a change of only a few degrees may be enough. However, the distance from the radiator to the edge has a large effect on the angular location of the maxima and minima and hence on the antenna gain. In the case of one dielectric sheet antenna manufactured in some quantity, the side lobes were maintained under 17 db below the main lobe by proper control of the dielectric thickness. A y-z plane pattern of this antenna is shown in Fig. 6; it is obtained only for the particular diffraction situation under which the unit was tested.

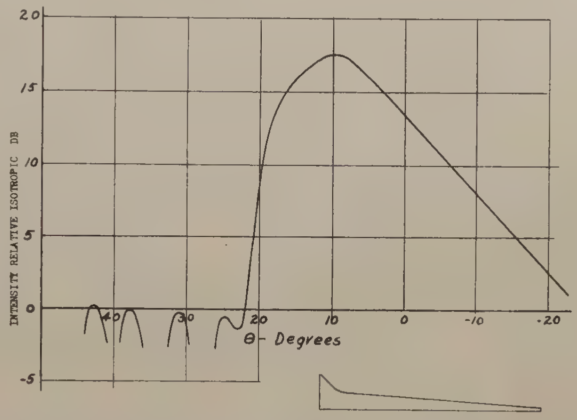

Fig. 6—Radiation pattern in y-z plane for 1×16-inch dielectric sheet antenna on plate 2 feet long. X band. Inset is dielectric profile.

The width of the dielectric sheet is also an important factor in the antenna performance. The dielectric sheet is easily fed from a wide angle sectoral horn because the dielectric can be formed to include the correcting lens needed in the mouth of the horn.

DIELECTRIC SHEET ANTENNA PERFORMANCE

Figs. 7–13 (following pages) show y-z plane patterns for a series of dielectric sheet radiators $2\frac{3}{8}$ inches wide made from G-7 Silicone Fiberglass and located at one end of a 4-foot flat plate. The radiated electric vector lies in the y-z plane. Fig. 7 is the result for a 9-inch long sheet tapered for maximum gain. The remaining patterns are for various uniform thickness extensions to this original radiator. They are not, therefore, patterns for maximum gain profiles or for reduced side-lobe profiles. They illustrate the gross effects of antenna length and thickness on performance. The extension thicknesses are 1/32 inch for Figs. 8, 9, and 10.

These patterns were all measured at a distance of 40 feet and as a result are quite accurate for angles below 30 degrees. Fig. 7 shows the typical diffraction characteristics of greatest gain at a small angle on the radiator side of the plate, and small variations in level at greater angles. Minima at 13, 19, 23, and 27 degrees, are diffraction minima. In Fig. 8 the diffraction minima are evident as well as a new minimum at 19 degrees which results from the pattern of the 16-inch radiator. In Fig. 9 this minimum has moved to about 15 degrees, and in Fig. 10 to 13 degrees.

---

[10] E. C. Jordan, "Electro-Magnetic Waves and Radiating Systems," Prentice-Hall, Inc., New York, N. Y., pp. 572–577; 1950.

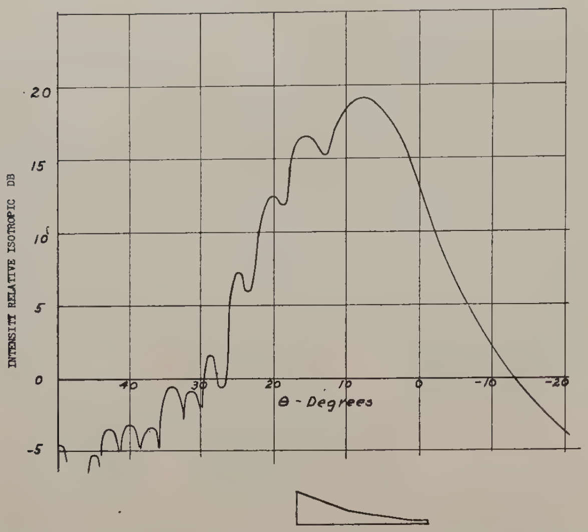

Fig. 7—Radiation pattern in y-z plane for $2\frac{3}{8}\times 9$-inch dielectric sheet antenna on 4-foot long plate. X band. Inset is dielectric profile.

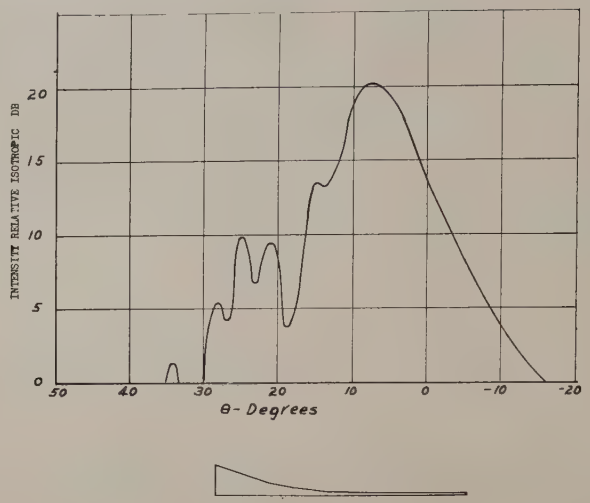

Fig. 8—Radiation pattern in y-z plane for $2\frac{3}{8}\times 17$-inch dielectric sheet antenna on 4-foot long plate. X band. Inset is dielectric profile.

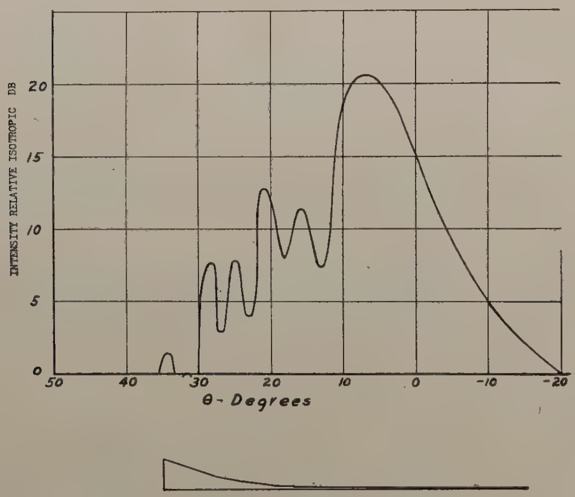

Fig. 9—Radiation pattern in y-z plane for $2\frac{3}{8}\times 25$-inch dielectric sheet antenna on 4-foot long plate. X band. Inset is dielectric profile.

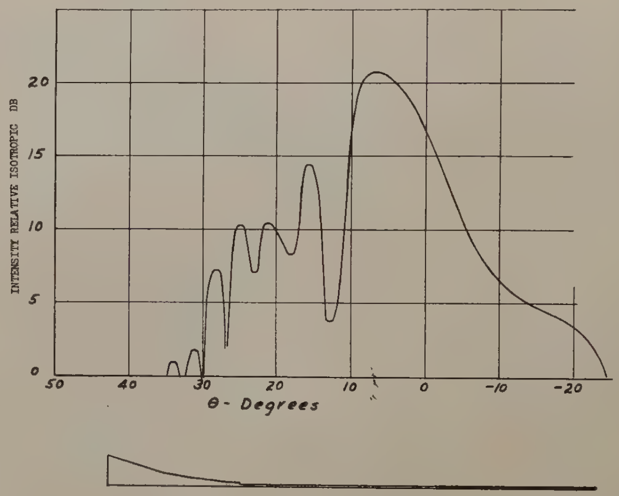

Fig. 10—Radiation pattern in y-z plane for $2\frac{3}{8}\times 33$-inch dielectric sheet antenna on 4-foot long plate. X band. Inset is dielectric profile.

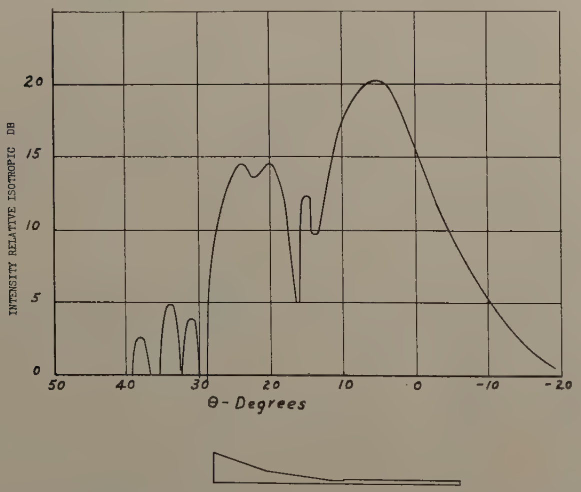

Fig. 11—Radiation pattern in y-z plane for $2\frac{3}{8}\times 17$-inch dielectric sheet antenna on 4-foot long plate. X band. Inset is dielectric profile.

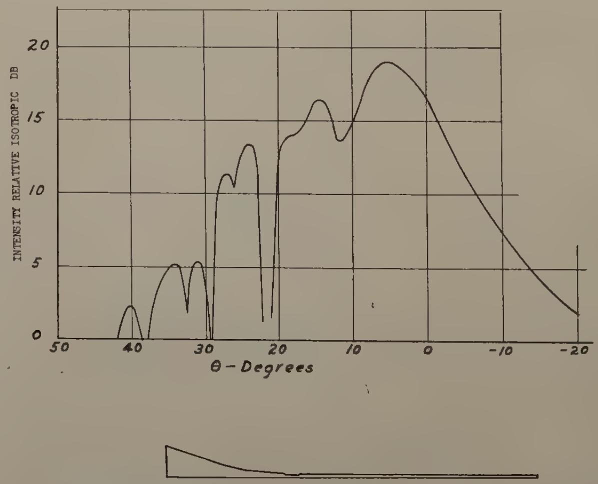

Fig. 12—Radiation pattern in y-z plane for $2\frac{3}{8}\times 25$-inch dielectric sheet antenna on 4-foot long plate. X band. Inset is dielectric profile.

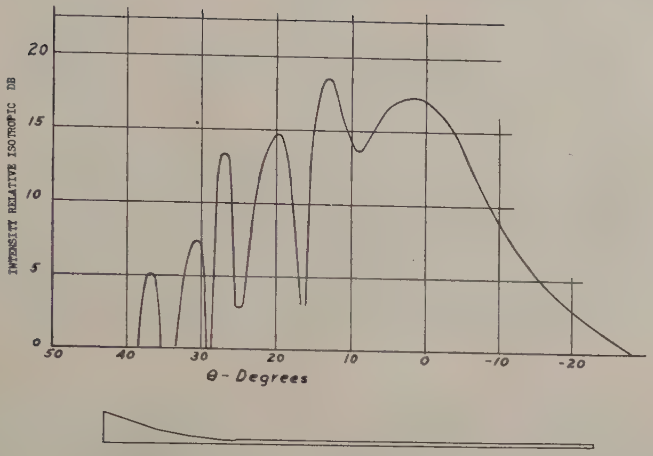

Fig. 13—Radiation pattern in y-z plane for $2\frac{3}{8}\times 33$-inch dielectric sheet antenna on 4-foot long plate. X band. Inset is dielectric profile.

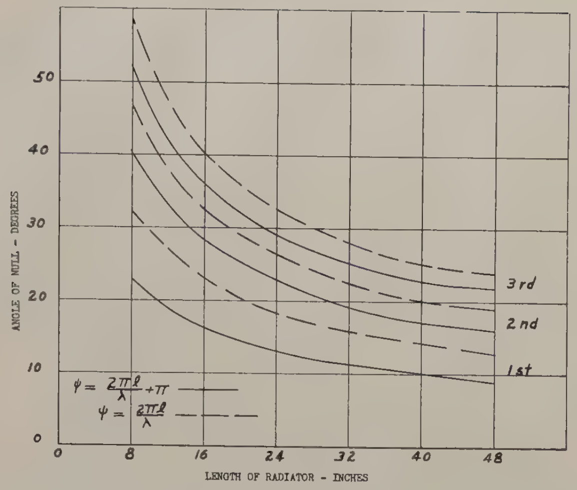

Fig. 14—Angular location of first three minima in radiation patterns of end fire arrays. ψ is total phase shift along array.

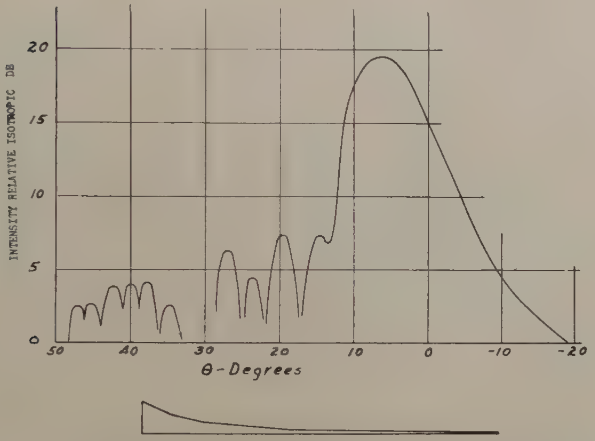

Fig. 15—Radiation pattern in y-z plane for $2\frac{3}{8}\times 24$-inch dielectric sheet antenna on 4-foot long plate. X band. Inset is dielectric profile.

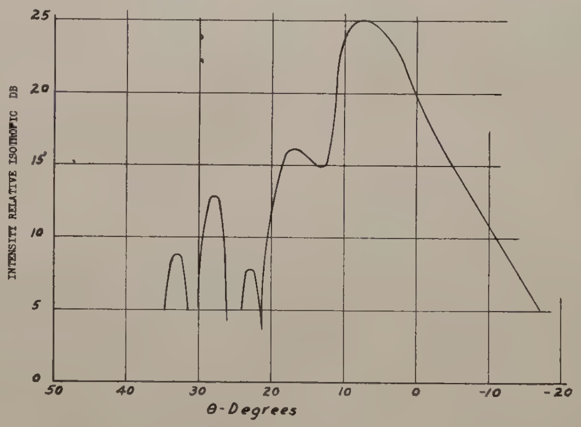

Fig. 16—Radiation pattern in y-z plane for 10×24-inch dielectric sheet antenna on 4-foot long plate and fed by a 60-degree horn and correcting lens. X band.

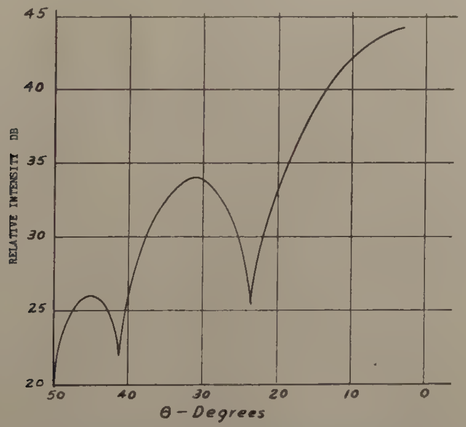

Fig. 17—Radiation pattern in y-z plane for $2\frac{3}{8}\times 9$-inch corrugated surface antenna on 4-foot long surface. Measured at 4 feet. X band.

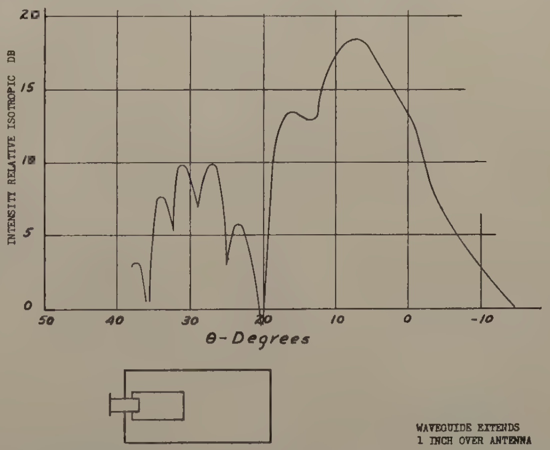

Fig. 18—Radiation pattern in y-z plane for $2\frac{3}{8}\times 9$-inch corrugated surface antenna on 4-foot long plate. Measured at 40 feet. X band.

Fig. 14 gives the location of the first three minima in the patterns of uniform and fire antennas for two phase shift conditions. The phase shift in the radiators of Fig. 7 to Fig. 10 is somewhere between these two limits.

Figs. 11 to 13 are patterns for $\frac{1}{16}$-inch extensions of the basic radiator. The change of null position with change in length is evident, as well as the fact that the side-lobe level is high. This thickness is excessive since the phase delay exceeds the maximum gain value.

The side-lobe structure of these patterns is a function of the fine details of the dielectric thickness profile. In particular the two most prominent side lobes of Fig. 10 can be reduced to 12 db below the main lobe at the expense of about 1 db of gain. This is accomplished by smoothing the profile and increasing the thickness slightly in the area between 5 and 10 inches from the feed end. Fig. 15 shows the resulting pattern.

Fig. 16 is the pattern for a 10-inch wide by 24-inch long antenna fed by a sectoral horn and dielectric lens. This unit is also on a 4-foot plate. No effort has been made to reduce side lobes, but the gain is near maximum. The dimensions of the sheet are nonuniform in the *X* direction. Some increase in gain is obtained by reducing the thickness of the sheet edges.

An evaluation of efficiency can be made for this unit. It has a beam approximately 9 degrees wide to half-power points in both x-z and y-z planes and a gain of about 300. This corresponds to efficiency of about 60 per cent. Efficiency is a real consideration for dielectric sheet transmission where the medium is not perfect. It is one of the factors limiting practical antenna lengths.

COMPARISON WITH CORRUGATED SURFACE RADIATORS

To establish a comparison with published work, the radiator reported by Ehrlich and Newkirk[4] (in their Fig. 17) was constructed. It was 10 inches long, $2\frac{3}{8}$ inches wide, with $16\frac{1}{32}$-inch $\times \frac{1}{8}$-inch slots per inch. It was mounted in a 4-foot plate. Fig. 17 is a near field pattern of this antenna. The first null was found at 23.5 degrees and the side-lobe level at -10 db. The far zone pattern is shown in Fig. 18 and is to be compared with Fig. 7, the pattern for a dielectric antenna of similar size. Greater phase delay is to be noted for the corrugated unit and nearly equal gain. A $\frac{1}{32}$-inch by 8-inch by $2\frac{3}{8}$-inch strip of dielectric placed on the metal surface at the end of the corrugated section increases the gain about 1 db just as it does for the dielectric sheet antenna.

CONCLUSIONS

Some characteristics of dielectric sheets as end fire radiators have been described. These properties are useful for some applications requiring simple antennas of small cross section. The dielectric sheet has much the same performance as corrugated surface antennas and somewhat simpler physical features.

THE NATURE OF FURTHER INVESTIGATION

Numerous aspects of the dielectric sheet require continued investigation. These include formal solution of the equations for finite-width sheets, measurements on sheets of nonuniform width and thickness, measurements on laminated sheets, and measurements on curved surface antennas.

The problem of matching to rigid waveguides also requires refinement and it is now receiving considerable attention.

Evaluation of Errors in an Eight-Element Adcock Antenna*

J. R. WAIT† AND W. A. POPE†

Summary—An analysis is given for the response of an eight-element direction finding antenna to a localized radio-frequency source. The error between the indicated and true bearing is evaluated and illustrated by graphs. It is also shown that the additional error, introduced by bringing the source into proximity of the antenna system is negligible if the antenna-source distance is greater than 5λ. This is an important consideration in the calibration of the system.

INTRODUCTION

THE ADVANTAGES of multi-element direction finding antenna systems over the conventional type employing four elements[1] have been pointed out first by Breuninger.[2] An analysis of fixed antennas with any number of elements was given by Redgment, Struszynski and Phillips.[3] They also discussed the merits of an eight element system, originally proposed by Rocke,[4] in which the adjacent elements are connected in parallel and are used in conjunction with a twin-channel receiver.

It is the purpose of this note to evaluate the error between the indicated bearing and the true bearing of a radio frequency source situated at some distant point. Curves are presented that illustrate the way in which the error varies with the true bearing, wavelength, geometry of the system, and distance to the source.

RESPONSE OF THE SYSTEM TO A DIPOLE SOURCE

The multi-element Adcock system is shown schematically in plan view [Fig. 1(a)]. Four pairs of identical vertical antennas are arranged symmetrically at a distance d about a fixed point 0. Each pair subtends an angle 2θ at 0. The source of a vertically polarized radio signal is located at P at a distance r_0 from 0 and its bearing angle is defined by ϕ_0. In usual operation r_0 is very much greater than d and it can be safely assumed that the antenna system is excited by a plane wave. For calibration purposes, however, the source is located in the neighborhood of the antenna system where the static and induction fields of the source also become significant. A more elaborate analysis is therefore required for this case.

The distances from the point P to the respective elements are given by

$$r_m = (r_0^2 + d^2 - 2dr_0 \cos\theta_m)^{1/2} \text{ and}$$

$$r_m' = (r_0^2 + d^2 - 2dr_0 \cos\theta_m')^{1/2} \text{ for } m = 1, 2, 3, 4,$$

and where

$$\begin{aligned} \theta_1 &= \phi_0 - \theta, & \theta_2 &= \phi_0 + 90° - \theta, \\ \theta_3 &= 180° + \theta - \phi_0, & \theta_4 &= 90° + \theta - \phi_0 \\ \theta_1' &= \phi_0 + \theta, & \theta_2' &= \phi_0 + 90° + \theta, \\ \theta_3' &= 180° - \theta - \phi_0, & \theta_4' &= 90° - \theta - \phi_0. \end{aligned} \tag{1}$$

The field at the mth receiving element due to the source at P is proportional to

$$r_m^{-3}(1 + i\beta r_m - \beta^2 r_m^2 F)e^{-i\beta r_m} \tag{2}$$

where $\beta = 2\pi/\lambda$ and λ is the free space wavelength.

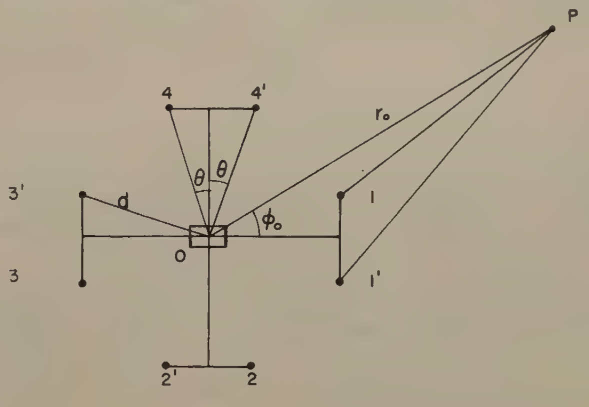

(a)

Fig. 1(a)—The eight-element Adcock system and the radio frequency source at P.

The term F is Norton's[5] surface wave attenuation factor which approaches unity for a highly conducting ground. In this analysis it is assumed that $F = 1$ corresponding to the case of a perfectly conducting flat ground.

The induced signals in the individual pairs are connected in parallel. The outputs of the four junction points are connected to the field coils of a two-phase goniometer shown schematically in Fig. 1(b).[6] The voltage E_{31}, which energizes the field coil a-c, is equal to the difference of the voltage outputs of the receiving element pairs 3, 3′ and 1, 1′. Similarly, the voltage E_{42}, which energizes the field coil b-d, is equal to the difference of the voltage outputs of the receiving element pairs 4, 4′ and 2, 2′.

The search coil, designated in Fig. 1(b) by e-f, is connected to a sensitive null detector. If the bearing of the

---

* Received by the PGAP, May 10, 1954; received by the IRE, July 7, 1954. This work was carried out under R.P.L. Project No. 28-0.

† Radio Phys. Lab., Defence Res. Bd., Ottawa, Can.

[1] R. H. Barfield and W. Ross, "A short-wave Adcock direction finder," *Jour. Inst. Elec. Engr.*, vol. 81, p. 682; 1937.
J. G. Holbrook, "An analysis of errors in long range radio direction finder systems," PROC. I.R.E., vol. 41, p. 1747; December, 1953.

[2] H. W. Breuninger, "Brauchbarkeitsgrenzen des n-Mast Adcock-Peilers," *Hochfrequenz. und Electroak.*, vol. 59, p. 50; 1942.

[3] P. G. Redgment, W. Struszynski, and G. J. Phillips, "Multi-aerial Adcock d.f. systems," *Jour. Inst. Elec. Engs.*, vol. 94, p. 751; 1951.

[4] British Patent Application No. 29088/45, Sir C. S. Wright, P. G. Redgment, A. F. L. Rocke.

[5] K. A. Norton, "Propagation of radio waves over the surface of the earth," PROC. I.R.E., vol. 25, p. 1203; September, 1937.

[6] The goniometer is assumed to have a high input impedance.

search coil is defined by Φ, the voltage output V at the terminals e-f is given by

$$V = A(E_{31} \cos \Phi - E_{42} \sin \Phi) \tag{3}$$

where A is a constant of the goniometer.

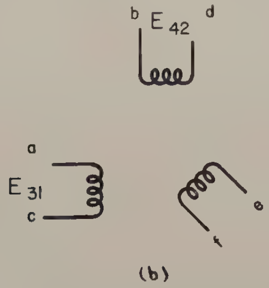

Fig. 1(b)—Schematic representation of the goniometer field coils (b–d and a–c) and search coil (e–f).

If the source P is at an infinite distance, E_{31} and E_{42} are in phase (or anti-phase) and the voltage V is then equal to zero when

$$\tan \Phi = \frac{E_{31}}{E_{42}}. \tag{4}$$

As the source P moves into the vicinity of 0, the voltages E_{31} and E_{42} are not in phase and there is no goniometer bearing Φ where V is identically zero. This corresponds to the case of an elliptically polarized magnetic field being excited in the goniometer. It is anticipated, however, that for cases of practical interest, the phase difference between E_{31} and E_{42} is small if $r_0/d > 10$. From considerations of the geometry of the ellipse it can then be easily deduced that the search coil voltage V will be a minimum when $\Phi = \phi$, where

$$\tan \phi = \left| \frac{E_{31}}{E_{42}} \right| \tag{5}$$

where ϕ is defined as the indicated bearing. The "sharpness" of the indicated bearing is characterized by the ratio K of the minimum to maximum values of V. This ratio K is also equal to the ratio of the minor to major axes of the magnetic field in the goniometer, and again from geometrical considerations it can be deduced that

$$K = \tfrac{1}{2} \tan \psi \sin 2\phi_0 \tag{6}$$

where K has been assumed small compared to unity and ψ is defined by

$$\frac{E_{31}}{E_{42}} = \left| \frac{E_{31}}{E_{42}} \right| e^{i\psi}. \tag{7}$$

The formulas for the indicated bearing angle ϕ and the phase term ψ are then given by

$$\tan \phi = \left[\frac{X^2 + Y^2}{U^2 + V^2} \right]^{1/2} \quad \text{and} \quad \psi = \tan^{-1} \frac{Y}{X} - \tan^{-1} \frac{V}{U}$$

where

$$\begin{aligned} X &= A(\alpha_1) + A(\alpha_1') - A(\alpha_3) - A(\alpha_3') \\ Y &= B(\alpha_1) + B(\alpha_1') - B(\alpha_3) - B(\alpha_3') \\ U &= A(\alpha_2) + A(\alpha_2') - A(\alpha_4) - A(\alpha_4') \\ V &= B(\alpha_2) + B(\alpha_2') - B(\alpha_4) - B(\alpha_4') \end{aligned} \tag{8}$$

where

$$\begin{aligned} A(\alpha_m) &= \alpha_m^{-3}\left[(1 - \alpha_m^2) \cos \alpha_m + \alpha_m \sin \alpha_m\right] \\ B(\alpha_m) &= \alpha_m^{-3}\left[\alpha_m \cos \alpha_m - (1 - \alpha_m^2) \sin \alpha_m\right] \end{aligned}$$

and

$$\alpha_m = \beta r_m = 2\pi r_m/\lambda.$$

When the ratio r_0/d approaches infinity the expressions for $\tan \phi$ and ψ simplify considerably to

$$\tan \phi = \frac{\sin (2\pi d\lambda^{-1} \sin \phi_0 \cos \theta) \cos (2\pi d\lambda^{-1} \cos \phi_0 \sin \theta)}{\sin (2\pi d\lambda^{-1} \cos \phi_0 \cos \theta) \cos (2\pi d\lambda^{-1} \sin \phi_0 \sin \theta)} \tag{9}$$

and $\psi = 0$.

The bearing error Δ is now defined by

$$\Delta = \phi - \phi_0$$

being the difference between the true bearing and the indicated bearing. It is quite apparent that the error Δ is octantal in nature. It is, therefore, only necessary to carry out calculations for ϕ_0 ranging from 0 to 45 degrees. It must be remembered, however, that the sign of Δ changes as ϕ_0 passes through every 45 degrees, since Δ is an odd function about the 45 degree bearing points.

PRESENTATION OF RESULTS

The bearing error Δ for the case $r_0/d = \infty$ has been calculated from (9) for a range of values of the relative spacing d/λ, the bearing ϕ_0, and the angle θ which specifies the shape of the array. These results (Figs. 2, 3, 4, page 161) are for θ values of 26.5, 27.5 and 30 degrees. The maximum bearing error Δ_m is then plotted in Fig. 5, page 161, as a function of d/λ for θ values of 0, 25, 26.5, 27.5, and 30 degrees.

In all cases it is seen that bearing error becomes large as d/λ approaches $\frac{1}{2}$. The maximum bearing error always occurs for values of ϕ_0 between 20 and 25 degrees. It is seen that for small values of d/λ ($<.2$) the optimum value of θ would be 30 degrees. This fact also is evident if (9) is rewritten in the following form:

$$\tan \phi \cong \tan \phi_0 \left[1 + \frac{1}{6} \left(2\pi \frac{d}{\lambda} \right)^2 \cos 2\phi_0 (\cos^2 \theta - 3 \sin^2 \theta) \right].$$

where terms of order $(d/\lambda)^4$ and higher have been neglected. It then follows that the coefficient of $(d/\lambda)^2$ term in the expansion is zero if $\theta = 30$ degrees.

For larger values of d/λ it appears that a smaller value of θ would be preferable. Using a different approach, Redgment *et al.*[3] have found the optimum value of θ to be 27.5, which is in accord with the results shown in Fig. 5. It should be pointed out, however, that their

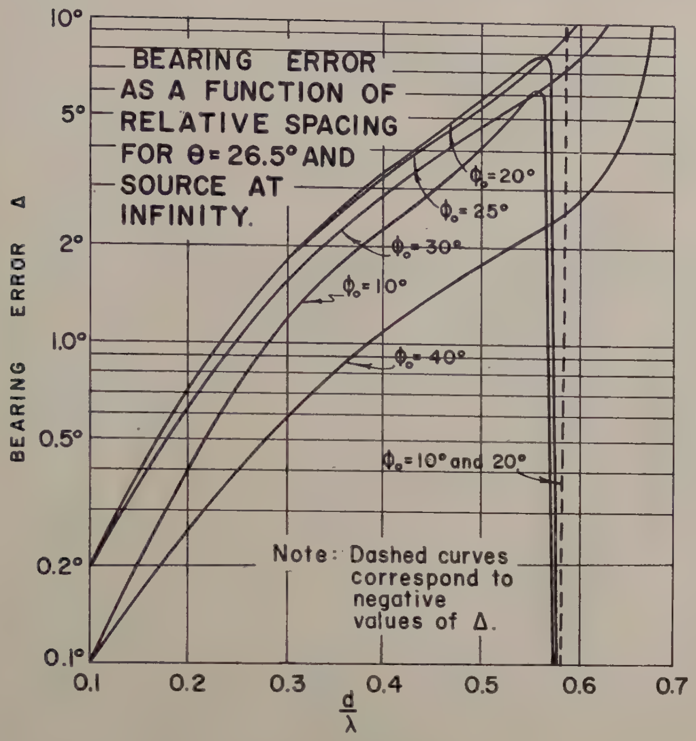

Fig. 2

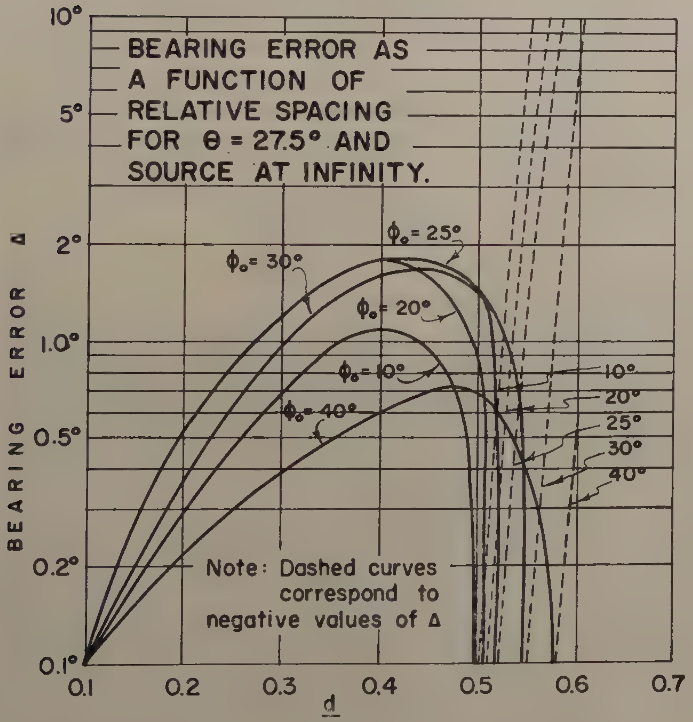

Fig. 3

results are not accurate for d/λ greater than about 0.4 since an approximate formula was used in place of (9).

While the computations for the case $r_0/d = \infty$ are very straightforward, this is not so for the case when r_0/d becomes finite. The error is plotted in Figs. 6, 7, and 8, on the following page, as a function of ϕ_0 for values of r_0/d of 10, 30, and 100 respectively. For sake of comparison, the corresponding value of Δ for $r_0/d = \infty$ are shown by

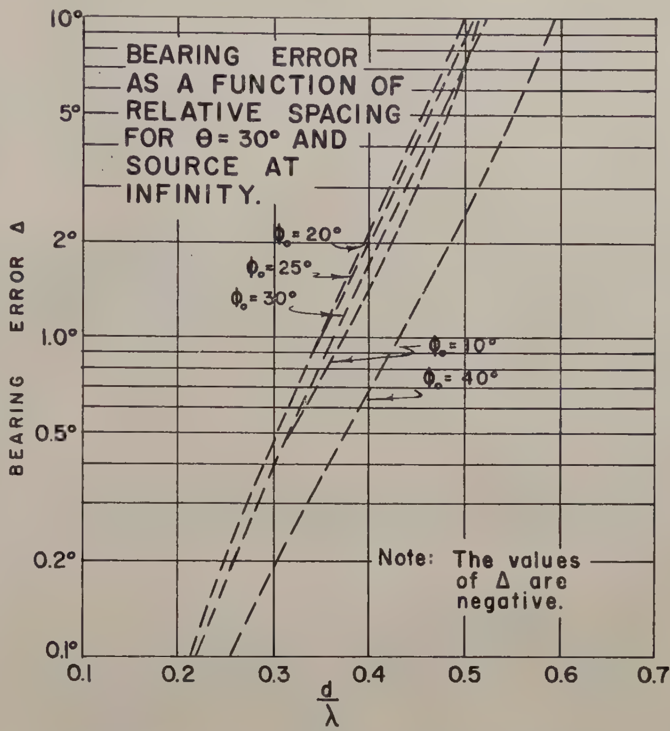

Fig. 4

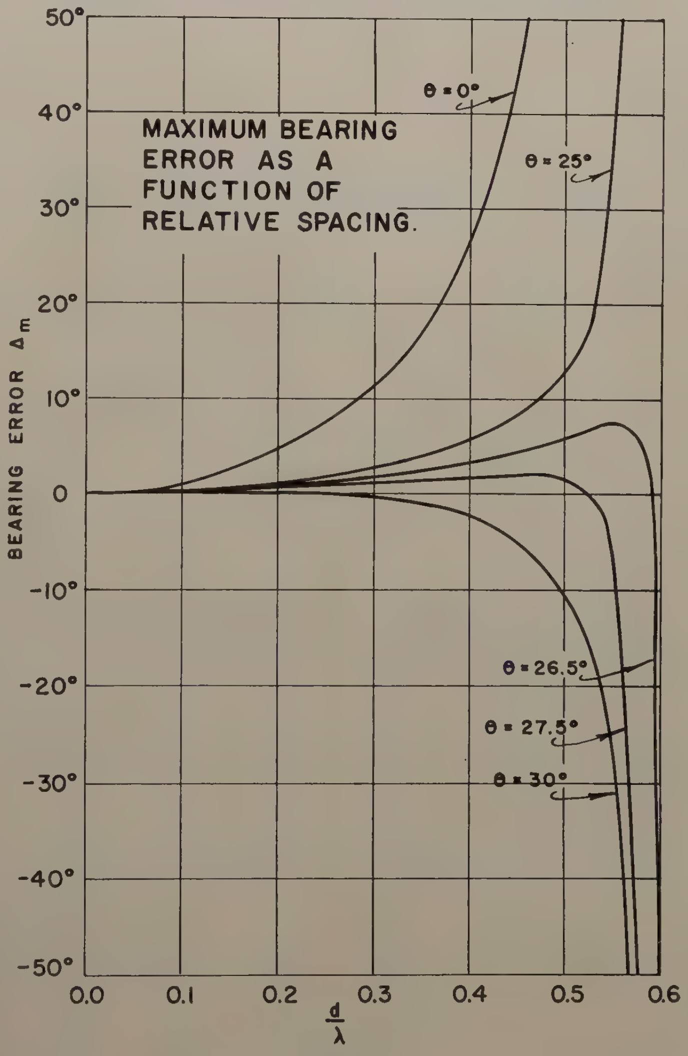

Fig. 5

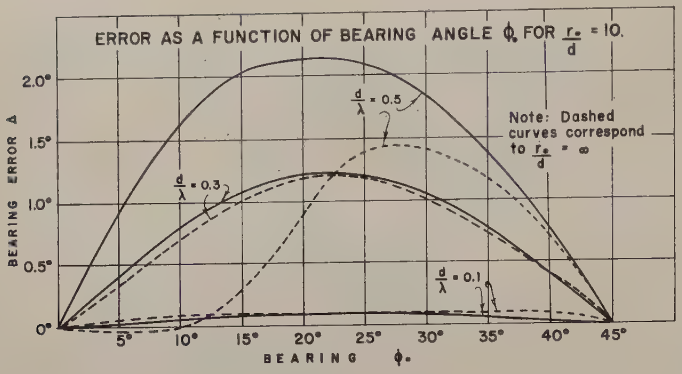

Fig. 6

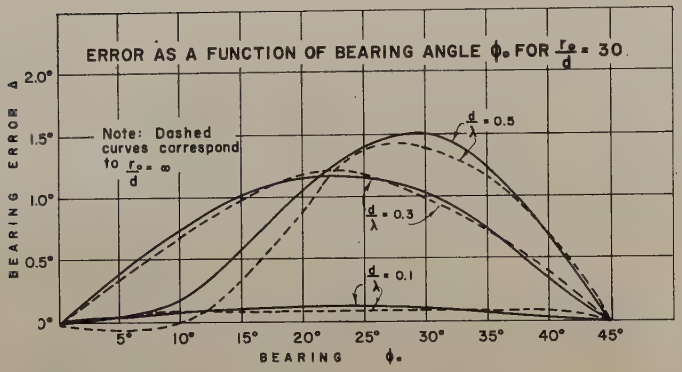

Fig. 7

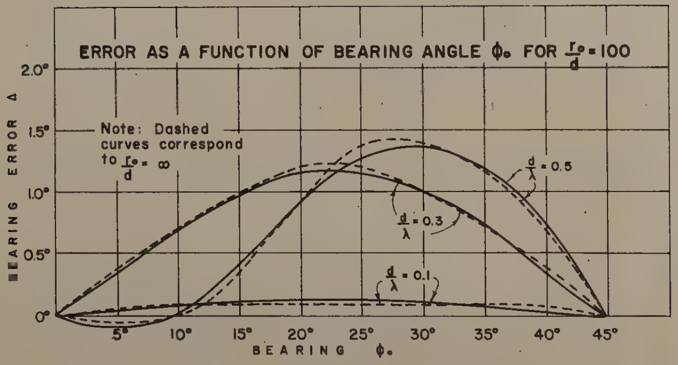

Fig. 8

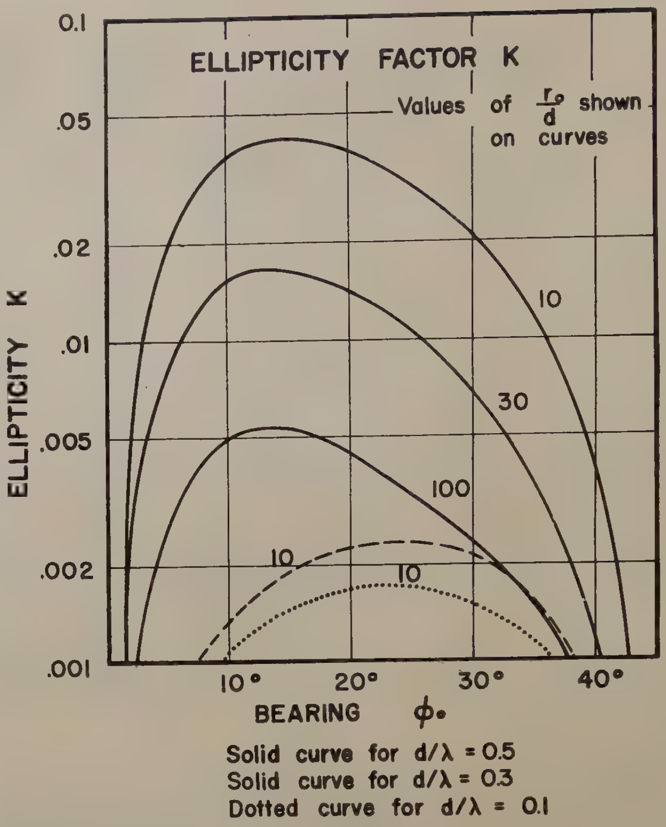

Fig. 9

the dashed curves. These results are believed to be accurate to less than $\frac{1}{20}$ of a degree. The difference between the solid and the dashed curves represents the calibration or proximity error δ.

The maximum value of δ appears to be always less than 1 degree except for the case $d/\lambda = 0.5$ and $r_0/d = 10$, where it is nearly 2 degrees.

The ellipticity factor K is plotted in Fig. 9 as a function of ϕ_0 for values of d/λ of 0.1, 0.3, and 0.5 respectively. It is seen that the maximum value of K is approximately 0.05 for the case $d/\lambda = 0.5$, $r_0/d = 10$ and $\phi_0 \approx 22$ degrees.

CONCLUSIONS

While this analysis has not been exhaustive, the results obtained should be useful for an estimation of the bearing error for any reasonable location of the radio-frequency source. In particular, the calculations indicate that the *additional error*, introduced by bringing the source into the proximity of the antenna system is negligible if the distance r_0 is greater than about 5λ at the maximum operating frequency (i.e. $d/\lambda \approx 0.5$). Another important consideration is the resulting ellipticity of the field in the goniometer when the source is in proximity to the antenna system. The indicated null then becomes broad, and difficulty might be encountered in obtaining an accurate measurement.

ACKNOWLEDGEMENT

This problem was proposed by C. W. McLeish and A. F. L. Rocke of the National Research Council of Canada. F. T. Davies and W. Searle also made several useful suggestions at the outset of this work.

* * *

communications

CORRESPONDENCE

The editors of the PGAP Transactions have recently received a letter[1] from Yasuto Mushiake, Faculty of Engineering, Tôhoku University, Sendai, Japan, on "An Exact Step-Up Impedance-Ratio Chart of a Folded Antenna," which is reproduced in its entirety as follows:

"The charts or nomographs[2,3] for the step-up impedance-ratio U of a folded antenna have usually been calculated from the approximate expression

$$a \simeq \log \frac{d}{\rho_1} \Big/ \log \frac{d}{\rho_2}, \tag{1}$$

and

$$U = (1 + a)^2, \tag{2}$$

where ρ_1 and ρ_2 are the radii of two conductors, and d is the spacing between them as illustrated in Fig. 1.

"However, (1) is applicable only when ρ_1 and ρ_2 are negligibly small compared with the spacing d. Otherwise we must use the following relation instead of (1), i.e.

$$a = \cosh^{-1}\left(\frac{d^2+\rho_1^2-\rho_2^2}{2d\rho_1}\right) \Big/ \left(\cosh^{-1}\left(\frac{d^2-\rho_1^2+\rho_2^2}{2d\rho_2}\right)\right). \tag{3}$$

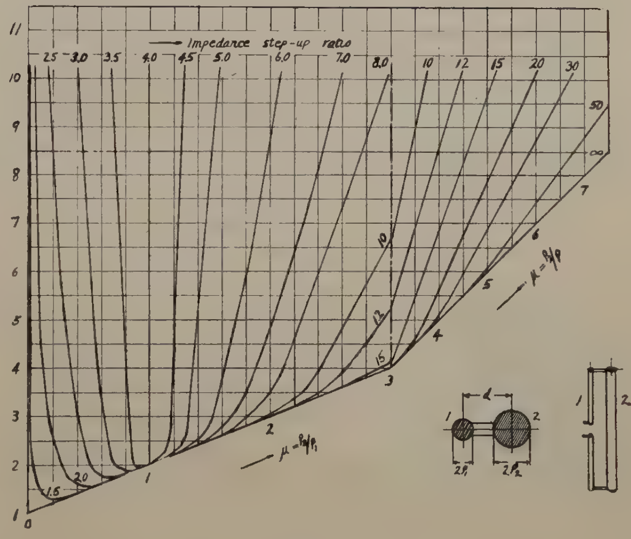

Fig. 1

The value of the step-up U calculated from (2) and (3) gives an exact one, in whatever relations these dimensions may be, so long as the dimensions of d, ρ_1 and ρ_2 are very small compared with the wavelength. In this meaning the exact numerical values of the step-up ratio are calculated, and a new chart is constructed with them as shown in Fig. 1."

* * *

---

[1] Received by the PGAP, April 26, 1954; received by the IRE, July 7, 1954.

[2] A.R.R.L., Antenna Book, 1949; p. 102.

[3] R. Guertler, "Impedance transformation in folded dipoles," *Jour. Brit. IRE*, vol. 9, pp. 344–350; September, 1949.

Transactions of the IRE
Professional Group on Antennas and Propagation

Index to Volume AP-2—1954

Contents

Volume AP-2, Number 1, January, 1954

Index Number *Page*
News and Views 1
1. UHF Omnidirectional Antenna Systems for Large Aircraft, W. Sichak and J. J. Nail 6
2. A Preliminary Survey of Tropospheric Refractive Index Measurements for U. S. Interior and Coastal Regions, C. M. Crain, J. R. Gerhardt and C. E. Williams 15
3. Some Stochastic Problems in Wave Propagation—Part I, Joseph Feinstein 23
4. A Preliminary Study of Fading of 100 Megacycle FM Signals, R. L. Riddle and C. R. Ammerman 30
5. VHF Field Intensities in the Diffraction Zone, R. N. Ghose and W. G. Albright 35
6. Mutual Impedance of Stacked Rhombic Antennas, J. G. Chaney 39

Volume AP-2, Number 2, April, 1954

Why Transactions? (Editorial) 41
News and Views 42
7. An Experimental Investigation of the Single-Wire Transmission Line, T. E. Roberts, Jr. 46
8. Sweep Frequency Backscatter—Some Observations and Deductions, Richard Silberstein 56
9. Some Stochastic Problems in Wave Propagation—Part II, Joseph Feinstein 63
10. On the Theory of Corrugated Plane Surfaces, R. S. Elliott 71
11. Meteoric Radio Echoes, L. A. Manning 82

Volume AP-2, Number 3, July, 1954

News and Views 91
12. Virtual Source Luneberg Lenses, G. D. M. Peeler, K. S. Kelleher, and H. P. Coleman 94
13. A Theoretical and Experimental Study of the Recombination Coefficient in the Lower Ionosphere, A. P. Mitra and R. E. Jones 99
14. Low Frequency Waves on Transmission Lines of Composite Section, R. W. Klopfenstein 103
15. Arrays of Closely-Spaced Nonresonant Slots, R. J. Stegen and R. H. Reed 109
16. A New Antenna Feed Having Equal E- and H-Plane Patterns, Alvin Chlavin 113
17. Paraboloid Reflector and Hyperboloid Lens Antennas, E. M. T. Jones 119

Volume AP-2, Number 4, October, 1954

News and Views 129
18. Analysis of Helical Transmission Lines by Means of the Complete Circuit Equations, V. J. Fowler 132
19. Radiation from a Vertical Dipole over a Stratified Ground, J. R. Wait and W. C. G. Fraser 144
20. A Waveguide Array for Solar Noise Studies, H. Gruenberg 147
21. Dielectric Sheet Radiators, F. E. Butterfield 152
22. Evaluation of Errors in an Eight-Element Adcock Antenna, J. R. Wait and W. A. Pope 159

Communications:

23. An Exact Step-Up Impedance-Ratio Chart of a Folded Antenna, Y. Mushiake 163

Index to Authors

Numbers refer to index numbers in contents listing.

A
Albright, W. G.: 5
Ammerman, C. R.: 4

B
Butterfield, F. E.: 21

C
Chaney, J. G.: 6
Chlavin, A.: 16
Coleman, H. P.: 12
Crain, C. M.: 2

E
Elliott, R. S.: 10

F
Feinstein, J.: 3, 9
Fowler, V. J.: 18
Fraser, W. C. G.: 19

G
Gerhard, J. R.: 2
Ghose, R. N.: 5
Gruenberg, H.: 20

J
Jones, E. M. T.: 17
Jones, R. E.: 13

K
Kelleher, K. S.: 12
Klopfenstein, R. W.: 14

M
Manning, L. A.: 11
Mitra, A. P.: 13
Mushiake, Y.: 23

N
Nail, J. J.: 1

P
Peeler, G. D. M.: 12
Pope, W. A.: 22

R
Reed, R. H.: 15
Riddle, R. L.: 4
Roberts, T. E., Jr.: 7

S
Sichak, W.: 1
Silberstein, R.: 8
Stegan, R. J.: 15

W
Wait, J. R.: 19, 22
Williams, C. E.: 2

Index to Technical Subjects

Adcock Antenna Error Evaluation: 22
Aircraft Antennas, Omnidirectional: 1
Antenna Feed with Equal *E* and *H* Plane Patterns: 16
Backscatter Observations, Sweep-Frequency Method: 8
Corrugated Plane Surface: 10
Dielectric Sheet Radiators: 21
Dipole Radiation over Stratified Ground: 19
Fading of 100 Mc FM Signals: 4
Field Intensities in Diffraction Zone, VHF: 5
Folded Antenna Impedance Chart: 23
Helical Transmission Line Analysis: 18
Hyperboloid Lens: 17
Lens, Luneberg: 12
Meteoric Radio Echoes, Survey: 11
Paraboloid Reflector: 17
Recombination Coefficient in Lower Ionosphere: 13
Refractive Index Measurements, U. S.: 2
Rhombic Antennas, Mutual Impedance: 6
Single-Wire Transmission Line Experiments: 7
Slots, Closely-Spaced: 15
Stochastic Problems in Wave Propagation: 3, 9
Transmission Lines of Composite Section: 14
VHF Field Intensities in Diffraction Zone: 5
Waveguide Array for Solar Noise Studies: 20

Nontechnical Index

Editorials

"Why Transactions," by Ernst Weber: March, p. 41

Group News

Administrative Committee: July, p. 91; October, pp. 129, 130
Chapters:
  Albuquerque-Los Alamos: January, p. 3; March, p. 44; July, p. 92
  Chicago: March, p. 44; October, p. 131
  Los Angeles: January, p. 4; July, p. 92
  San Diego: January, p. 3
  Washington: January, p. 3; July, p. 92
Subdivision: January, pp. 1–2; July, p. 92
Transactions: January, p. 2, 3; March, p. 45; July, pp. 91–92; October, p. 129

Meetings

IRE National Convention, 1954: January, pp. 3, 4
URSI Fall Meeting, 1953: January, p. 4
URSI Spring Meeting, 1954: March, p. 44
Western Electronics Convention, 1954: March, p. 44; July, p. 92

Miscellaneous

Antennas and Waveguide Committee: January, p. 3; July, p. 92
Combining Professional Groups: October, p. 129
Data on Professional Groups: October, p. 130
National Bureau of Standards Relocated: October, p. 130
New Unit for Logarithmic Ratios: pp. 42–44

Personals

Cohn, S.: October, p. 131
Jordan, E. C.: July, p. 93; October, p. 131
Loria, R. M.: October, p. 131
Newman, M. M.: October, p. 131
Rumsey, V. H.: July, p. 93

INSTITUTIONAL LISTINGS

The IRE Professional Group on Antennas and Propagation is grateful for the assistance given by the firms listed below, and invites application for Institutional Listing from other firms interested in the field of Antennas and Propagation.

THE GABRIEL LABORATORIES, Div. of the Gabriel Co., 135 Crescent Road, Needham Heights 94, Mass.
Research and Development of Antenna Equipment for Government and Industry.

HUGHES AIRCRAFT COMPANY, Culver City, California
Research, Development, Manufacture: Radar, Guided Missiles, Tubes, Systems, Solid State Physics, Computers.

MARYLAND ELECTRONIC MANUFACTURING CORPORATION, College Park, Maryland
Antenna and System Development and Production for Civil and Military Requirements.

I-T-E CIRCUIT BREAKER CO., Special Products Div., 601 E. Erie Ave., Philadelphia 34, Pa
Design, Development and Manufacture of Antennas and Related Equipment.

JANSKY & BAILEY, INC., 1339 Wisconsin Ave. N.W., Washington 7, D.C.
Radio & Electronic Engineering; Antenna Research & Propagation Measurements; Systems Design & Evaluation.

WHEELER LABORATORIES, INC., 122 Cutter Mill Road, Great Neck, New York
Consulting Services, Research and Development, Microwave Antennas and Waveguide Components.

ANDREW CORPORATION, 363 E. 75th Street, Chicago 19, Ill.
Development and Production of Antenna and Transmission Line Systems.

DORNE AND MARGOLIN, INC., 30 Sylvester Street, Westbury, L. I., New York
Antenna Research and Development—Radiation Pattern Measuring Services.

The charge for an Institutional Listing is $25.00 per issue or $75.00 for four consecutive issues. Application for listing may be made to the Technical Secretary, The Institute of Radio Engineers, 1 East 79th Street, New York 21, New York.